



Calhoun: The NPS Institutional Archive

Theses and Dissertations

Thesis Collection

1992-06

Current density limitations in a fast-pulsed high-voltage vacuum diode

Welsh, David S.

Monterey, California. Naval Postgraduate School

<http://hdl.handle.net/10945/23850>



Calhoun is a project of the Dudley Knox Library at NPS, furthering the precepts and goals of open government and government transparency. All information contained herein has been approved for release by the NPS Public Affairs Officer.

Dudley Knox Library / Naval Postgraduate School
411 Dyer Road / 1 University Circle
Monterey, California USA 93943

<http://www.nps.edu/library>

REPORT DOCUMENTATION PAGE

Form Approved
OMB No 0704-0188

1a REPORT SECURITY CLASSIFICATION Unclassified		1b RESTRICTIVE MARKINGS	
2a SECURITY CLASSIFICATION AUTHORITY		3 DISTRIBUTION/AVAILABILITY OF REPORT Approved for public release; distribution is unlimited.	
2b DECLASSIFICATION/DOWNGRADING SCHEDULE		5 MONITORING ORGANIZATION REPORT NUMBER(S)	
4 PERFORMING ORGANIZATION REPORT NUMBER(S)		7a. NAME OF MONITORING ORGANIZATION Naval Postgraduate School	
6a. NAME OF PERFORMING ORGANIZATION Naval Postgraduate School	6b OFFICE SYMBOL (If applicable) 33	7b ADDRESS (City, State, and ZIP Code) Monterey, CA 93943-5000	
6c ADDRESS (City, State, and ZIP Code) Monterey, CA 93943-5000		9 PROCUREMENT INSTRUMENT IDENTIFICATION NUMBER	
8a NAME OF FUNDING/SPONSORING ORGANIZATION	8b OFFICE SYMBOL (If applicable)	10 SOURCE OF FUNDING NUMBERS	
8c ADDRESS (City, State, and ZIP Code)		PROGRAM ELEMENT NO	PROJECT NO
		TASK NO	WORK UNIT ACCESSION NO
11 TITLE (Include Security Classification) CURRENT DENSITY LIMITATIONS IN A FAST-PULSED HIGH-VOLTAGE VACUUM DIODE			
12. PERSONAL AUTHOR(S) David S. Welsh			
13a TYPE OF REPORT Master's Thesis	13b TIME COVERED FROM _____ TO _____	14 DATE OF REPORT (Year, Month, Day) June 1992	15 PAGE COUNT 63
16 SUPPLEMENTARY NOTATION The views expressed in this thesis are those of the author and do not reflect the official policy or position of the Department of Defense or the U.S. Government.			
17 COSATI CODES		18 SUBJECT TERMS (Continue on reverse if necessary and identify by block number)	
FIELD	GROUP	current density ; cathode spot ; vacuum diode ; whisker ; unipolar arc ; space charge ; numerical ; simulation	
19 ABSTRACT (Continue on reverse if necessary and identify by block number) <p>An investigation into the limitations on the enhanced field-emitted current density in a fast-pulsed (rise-time on the order of ns), high voltage ($>10^6$ V), 1-inch vacuum diode was conducted using a computer simulation based on the Fowler-Nordheim equation.</p> <p>Oscillations in the emitted current density (due to the change in the amount of space charge within the gap) were found to quickly decay into a final steady-state for the voltages applied. Steady-state values for a wide variety of work functions, electric field enhancement factors (based on the theory that "whiskers" on the cathode surface experience varying degrees of enhancement), and applied potentials were compared to two benchmarks: the amount of current density required to explode a whisker in <10 ns by joule heating ($J_E = 10^9$ A/cm²); and the Child-Langmuir (C-L) space-charge-limited current density.</p>			
20 DISTRIBUTION/AVAILABILITY OF ABSTRACT <input checked="" type="checkbox"/> UNCLASSIFIED/UNLIMITED <input type="checkbox"/> SAME AS RPT <input type="checkbox"/> DTIC USERS		21. ABSTRACT SECURITY CLASSIFICATION Unclassified	
22a NAME OF RESPONSIBLE INDIVIDUAL F. Schwirzke		22b TELEPHONE (Include Area Code) (408) 646-2635	22c OFFICE SYMBOL PhSw

19. (cont)

Steady-state values were found to be less than J_E . One model of the formation process of a plasma at the cathode surface requires that J_E be met or exceeded by the steady-state value. Thus, such a model is not supported by this project's findings.

The C-L limit is based on a thermionic-type emission process. As only pure field emission (i.e., no thermionic emission included) was considered, the steady-state values were, in all conclusive cases, less than the corresponding C-L limited values.

Approved for public release: distribution is unlimited.

CURRENT DENSITY LIMITATIONS IN A FAST-PULSED HIGH-VOLTAGE VACUUM DIODE

by

D. S. Welsh

Lieutenant, United States Navy

B. S., Pennsylvania State University, 1986

Submitted in partial fulfillment of the
requirements for the degree of

MASTER OF SCIENCE IN PHYSICS

from the

NAVAL POSTGRADUATE SCHOOL

June 1992

ABSTRACT

An investigation into the limitations on the enhanced field-emitted current density in a fast-pulsed (rise-time \approx ns), high voltage ($> 10^6$ V), 1-inch vacuum diode was conducted using a computer simulation based on the Fowler-Nordheim equation.

Oscillations in the emitted current density (due to the change in the amount of space charge within the gap) were found to quickly decay into a final steady-state for the voltages applied. Steady-state values for a wide variety of work functions, electric field enhancement factors (based on the theory that "whiskers" on the cathode surface experience varying degrees of enhancement), and applied potentials were compared to two benchmarks: the amount of current density required to explode a whisker in < 10 ns by joule heating ($J_E = 10^9$ A/cm²); and the Child-Langmuir (C-L) space-charge-limited current density.

Steady-state values were found to be less than J_E . One model of the formation process of a plasma at the cathode surface requires that J_E be met or exceeded by the steady-state value. Thus, such a model is not supported by this project's findings.

The C-L limit is based on a thermionic-type emission process. As only pure field emission (i.e., no thermionic emission included) was considered, the steady-state values were, in all conclusive cases, less than the corresponding C-L limited values.

Table of Contents

I. INTRODUCTION	1
II. BREAKDOWN AND EMISSION THEORY	2
A. BACKGROUND	2
B. THE MODEL DIODE	4
C. ELECTRON EMISSION FROM THE CATHODE	5
D. NON-APPLICABILITY OF CHILD-LANGMUIR LAW	11
E. EXPLOSIVE MODEL CURRENT DENSITY REQUIREMENT	12
III. SIMULATION	13
A. BACKGROUND	13
B. SIMULATION THEORY	13
1. Electric Field	14
2. Equation of Motion	18
IV. RESULTS	19
A. OBJECTIVE	19
B. METHODS OF OBTAINING RESULTS	19
C. SIMULATION RESULTS	25
D. OTHER GRAPHICAL OUTPUT	27
V. CONCLUSIONS	41
APPENDIX A: DIMENSIONLESS VARIABLES	43
APPENDIX B: SIMULATION PROGRAM	47
LIST OF REFERENCES	55
INITIAL DISTRIBUTION LIST	56

ACKNOWLEDGEMENTS

This thesis research was quite a time-consuming task; competition from classwork, the occasional mental diversion, and the daily necessities such as eating, sleeping, etc., was often fierce. There was, however, one category of interference with which I was fortunate enough not to be hampered by my entire tour here at NPS-- routine daily admin.. These administrative details were handled cheerfully and with expertise by the educational technicians assigned to the Weapons Office, and I would like to express my gratitude to Jill, Eva, and Lori for their most invaluable contribution to this paper.

I would also like to thank Professor Schwirzke for taking me on as his student and introducing me to the physics of the unipolar arc. And finally I would like to thank Professor Colson for his valuable insights into the myriad of troubles I initially experienced with my simulation program; his guidance in these and other matters proved most beneficial.

I. INTRODUCTION

The breakdown of the surface of the cathode in a pulsed vacuum diode has been the subject of much investigation in recent years. The existence of crater-like cathode spots after breakdown can be explained by unipolar arcing, but the phenomena occurring prior to the arcing are still debated.

One model contends that a metallic "whisker" on the surface of the cathode provides a source for the enhanced emission of electrons. After a period of time (less than 10 ns for a fast-pulsed diode), the whisker explodes (due to the rapid build up of energy produced by the emission process) into a dense plasma which in turn drives the unipolar arc.

This project will attempt to show that field emission alone (i.e., not including thermionic emission) from a whisker cannot reach high enough values to trigger the explosion mechanism. A computer simulation utilizing the Fowler-Nordheim equation for field emission will be used. The results will also be compared to the well-known Child-Langmuir space-charge-limited current density for a vacuum diode.

A look at the dimensionless variables used in the program and the program itself are included in the appendices.

II. BREAKDOWN AND EMISSION THEORY

A. BACKGROUND

For over six decades scientists have been investigating pulsed-voltage vacuum diode breakdown. With the advent of newer technologies, shorter and shorter voltage-pulse rise times have become possible, with values ranging from 10^{-6} seconds in 1928 to 10^{-9} seconds today [Ref. 1]. Corresponding to today's very short rise times has been the discovery that breakdown even occurs on the nanosecond time scale. The effects of the breakdown process on the surface of the cathode have been well documented [Refs. 1-3], and a theory of the formation of cathode spots (Fig. 1) via unipolar arcing¹ has recently been proposed [Refs. 2,3]. In dispute, however, is the process by which the plasma driving the unipolar arc is formed.

Cathode spots are characterized by the formation of a dense quasi-neutral plasma near the cathode surface. There are two basic schools of thought concerning the primary mechanism for breakdown and the source of the plasma, only one of which will be attended to here. Anode-initiated breakdown would occur when ions released from the anode (due to bombardment of the anode by electrons emitted from the cathode) interact with the cathode to form the plasma. Here fast-pulse (\approx nanoseconds) breakdown shall be investigated, in which the anode-emitted ions would not have time to reach the cathode (for the 1 in = 2.54 cm diode gap of interest) before breakdown occurs; anode-initiated breakdown shall be discussed no further.²

¹ The concept of an arc which originates and terminates on the same surface (i.e., "unipolar") was first expounded by Robson and Thonemann in 1958, and was later expanded by Schwirzke in the 1980's [Refs. 2,4].

² For a more thorough treatment of anode-initiated breakdown, see [Ref. 1].

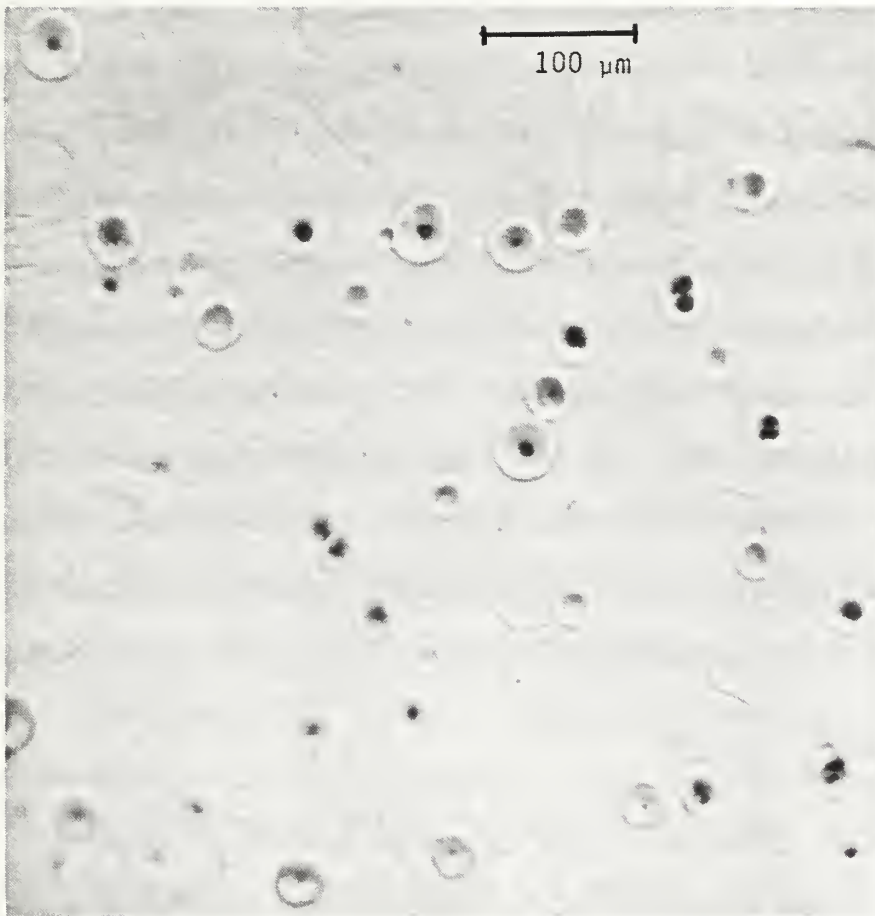


Figure. 1. Crater-like cathode spots formed by unipolar arcing.

In the cathode-initiated breakdown school, it is proposed that all of the ions and electrons which make up the plasma are produced by processes which are initiated by events occurring only at the cathode [Ref. 1]. Within this school, however, there are many camps, each with its own views on what processes do indeed occur, and which events really take place to initiate them. One of the more reknown camps is led by Schwirzke, who recently proposed that neutrals released from the surface of the cathode are ionized by the emitted electrons, thus forming a plasma near the cathode surface [Refs. 2,3]. Another is led by Dyke (et al)³ who proposed that joule heating of an electron emission site causes the site to vaporize, and in the process ions are created which allow the plasma to form [Ref. 1]. Here shall be examined a third camp, championed by Mesyats [Ref. 1], in which Dyke's theory is taken to its most extreme limit, that of an explosion of the emission site into a plasma directly. The goal is to show that an elementary version of a Mesyats-type "explosive" model cannot support breakdown on a time-frame indicative of fast-pulsed voltage vacuum diode breakdown.

B. THE MODEL DIODE

The model's anode and cathode will consist of two polished metal plates separated by a vacuum. Despite the polishing and the degassing effect of the vacuum, however, some small-scale "irregularities" will nevertheless exist on the surfaces of the plates. Weakly bound bits of dust, oxides, and non-metallic inclusions litter the cathode surface, providing excellent sites for the enhanced field emission of electrons [Ref. 2]. These so-called "whiskers" will vary in size and shape, with the more needle-like (height-to-base ratio $\gg 1$) metallic protrusions providing the most

³ See [Ref. 1] for a list of references on Dyke's experiments.

enhancement of the field emission. Flatter, non-metallic (e.g., dielectrics, semi-conductors, etc.) sites can also provide significant enhancement [Ref. 5].

C. ELECTRON EMISSION FROM THE CATHODE

There are two mechanisms for the electric-field-enhanced emission of electrons from a metallic surface: thermionic (high temperature, low applied field); and field (low temperature, high applied field) [Ref. 4]. The presence of the electric field at the surface lowers the potential barrier at the plate-vacuum interface, thus allowing electrons in the conduction band an opportunity to become free from the metal (Fig. 2). In thermionic emission, electrons at high temperatures gain enough kinetic energy to pass over the barrier and into the gap. In field emission, the electrons tunnel through the barrier instead. In general, the electric field at the emitter surface must be on the order of 10^7 V/cm for field emission to take place [Ref. 6]. For a diode gap of 2.54 cm (= 1 in), an applied potential of 2.54×10^7 V would be necessary to achieve field emission, but as noted previously, the whisker emission sites experience an enhanced applied electric field (Fig. 3). The enhancement factor, m , varies from 1 to several hundred, with needle-like whiskers having the largest values [Ref. 7]. For electric fields less than 10^7 V/cm, thermionic emission will dominate for temperatures above approximately 1500 K, with little substantial emission at lower temperatures [Ref. 6].

For the case of the non-metallic inclusions, a combination of field and thermionic emission occurs. Electrons tunnel from the metallic cathode material into the dielectric, then are thermionically emitted into the gap (see Fig. 4) [Ref. 5].

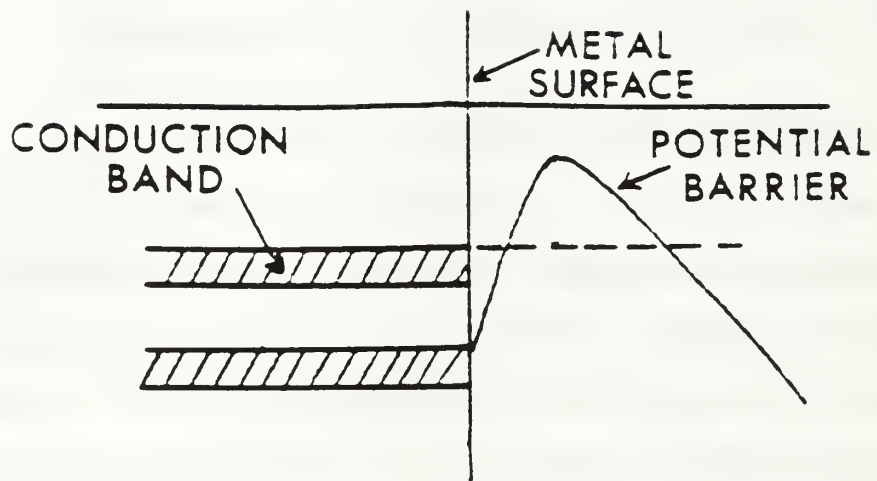


Figure 2. Lowering of potential barrier at metal-vacuum interface [Ref. 7].

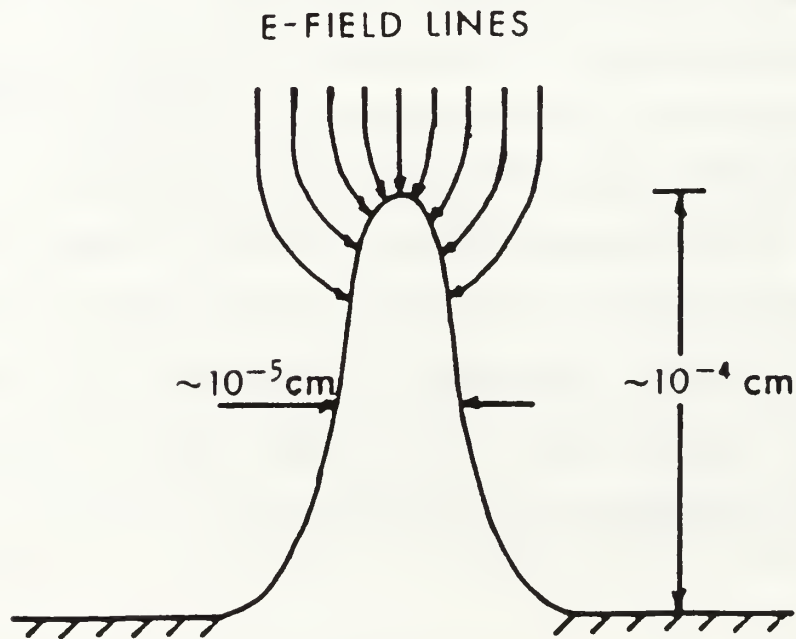


Figure 3. Enhancement of electric field at whisker tip [Ref. 7].

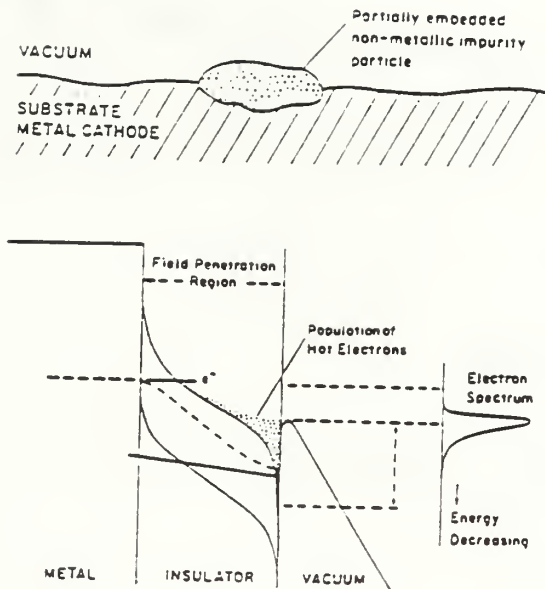


Figure 4. Combination of field and thermionic emission for a dielectric [Ref. 5].

For this elementary model, only field emission from metallic whiskers shall be considered, with the following assumptions:

1. The time-scale for the explosion of a whisker is only a few (≤ 10) nanoseconds;
2. The applied voltage rises instantaneously to a constant value at $t = 0$;
3. The gap is perfectly evacuated; no positive ions are present, so no heating of the site by ion bombardment is possible;
4. The initial temperature of the cathode (≈ 300 K) is too low for any appreciable amount of thermionic emission to occur at first; and
5. Any increase in temperature during the short time-frame prior to explosion shall be neglected (and thus so shall thermionic emission) in this elementary model.

Pure field emission is governed by the Fowler-Nordheim equation [Ref. 6]

$$J(F) = (1.54 \times 10^{-6}) \frac{F^2}{\phi} e^{(-6.83 \times 10^7) f(y) \frac{\phi^{3/2}}{F}}. \quad (1)$$

Since $f(y)$ (the Nordheim elliptic function) is slowly varying, it can be approximated as a constant⁴

$$f(y) \approx 0.94,$$

which leads to (see Figs. 5a,b)

$$J(F) = (1.54 \times 10^{-6}) \frac{F^2}{\phi} e^{(-6.42 \times 10^7) \frac{\phi^{3/2}}{F}}, \quad (2)$$

where

$J \equiv$ emitted current density (A/cm^2);

$F = -mE \equiv$ enhanced electric field⁵ at the whisker tip (V/cm);

$m \equiv$ electric field enhancement factor; and

$\phi \equiv$ work function of the cathode metal (eV).

J is a function only of F for any given whisker; any negative (i.e., electron) space charge which exists in the gap will reduce the emitted current density. If the applied potential remains constant, it can be predicted that J will start at some initial value, J_0 , and decrease as more and more space charge enters the gap. The electrons, once in the gap, will be accelerated across to the anode, eventually disappearing there. When the first emitted electrons reach the anode, the electric field at the cathode will increase due to the loss of space charge. The increased field will cause an increase

⁴ For a more thorough treatment of $f(y)$, see [Refs. 4,6].

⁵ Eq. (2) requires that F be defined as a positive quantity, hence the negative sign.

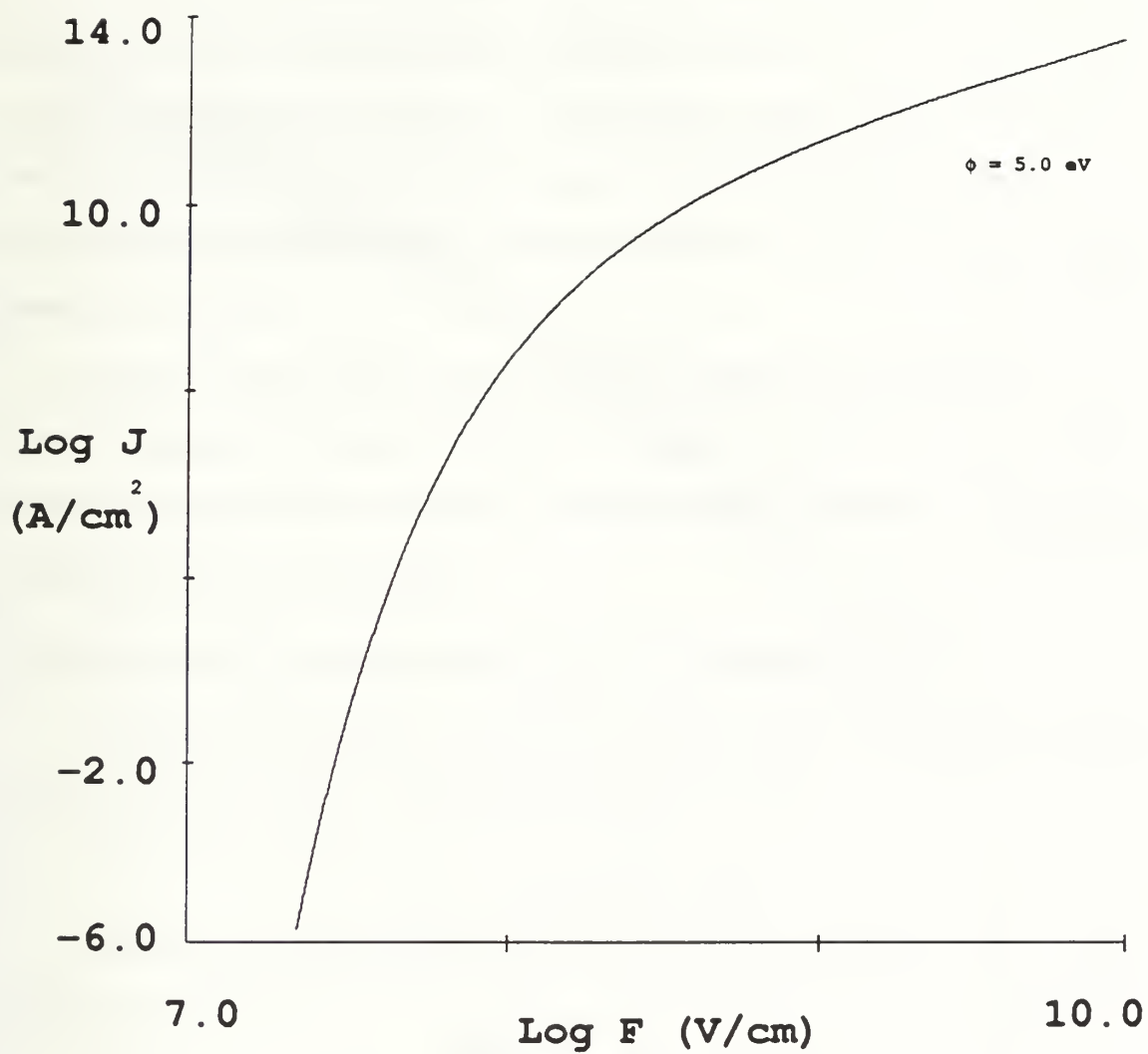


Figure 5a. Log plot of J vs. F (Eq. 2).

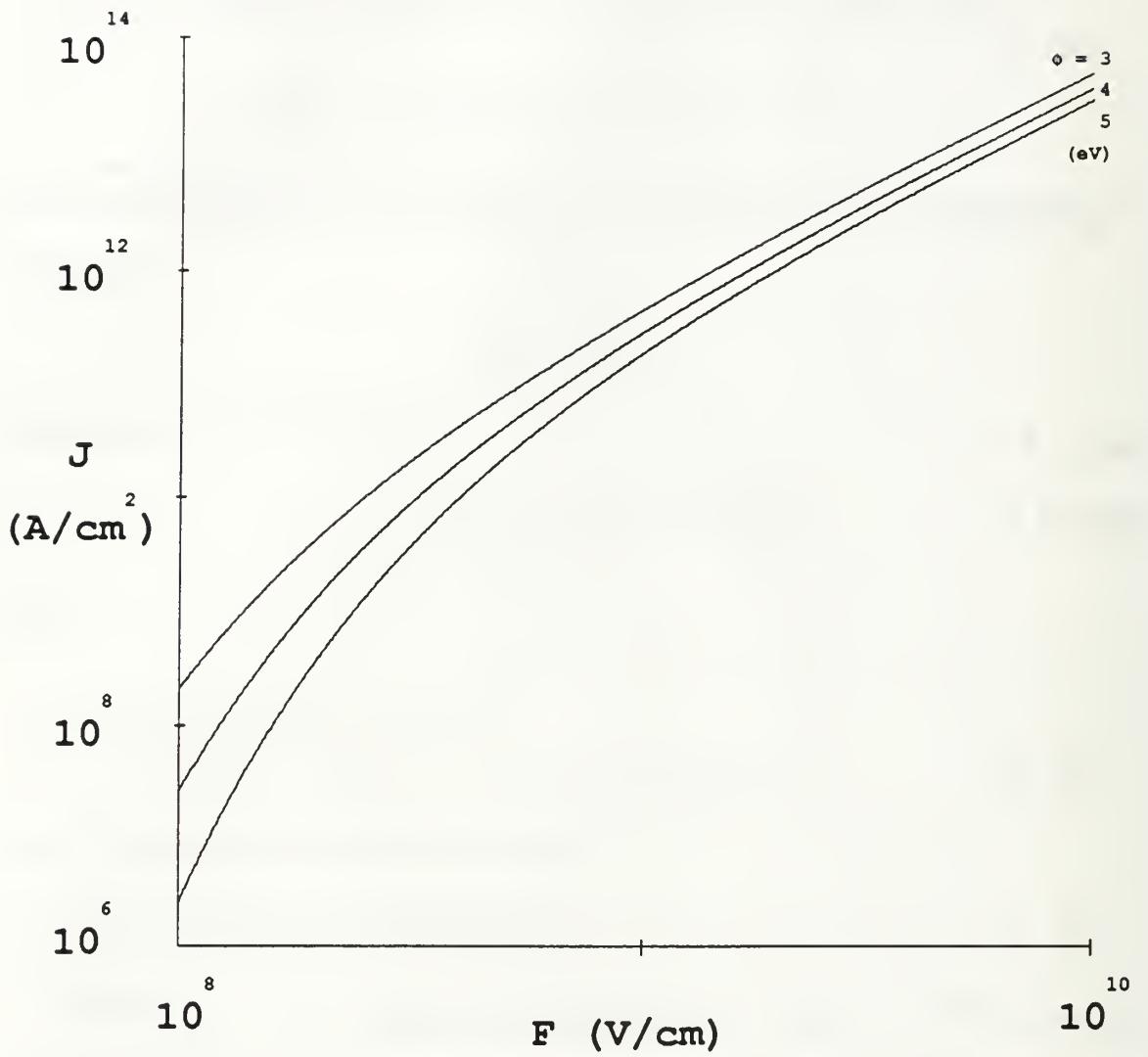


Figure 5b. Expanded log plot of J vs. F for various work functions (Eq. 2).

in J, but soon the increased addition of space charge will exceed the loss at the anode; the amount of space charge in the gap will then rise, the electric field at the cathode will decrease, and J will fall. This oscillatory action should diminish as the emitted current density at the cathode comes to equal that going into the anode. In other words, the current density becomes constant at some final space-charge-determined value, J_F .

It should be noted that in reality, the applied potential is not constant from $t = 0$. Rather, it ramps up from zero to some final value. The ramping has the effect of causing the current density to rise in a similar fashion; oscillations such as those described above are not observed.

D. NON-APPLICABILITY OF CHILD-LANGMUIR LAW

It is somewhat important to note, at this point, that J_F is *not* the well-known Child-Langmuir space-charge-limited current density (A/cm^2)

$$J_{CL} = \frac{4}{9} \epsilon_0 \left[\frac{2e}{M} \right]^{1/2} \frac{V^{3/2}}{d^2} , \quad (3)$$

with

$\epsilon_0 \equiv$ permittivity of free space $= 8.85 \times 10^{-12} \text{ C}^2/\text{N-m}^2$;

$e \equiv$ |electron charge| $= 1.60 \times 10^{-19} \text{ C}$;

$M \equiv$ electron mass $= 9.11 \times 10^{-31} \text{ kg}$;

$V \equiv$ applied voltage (V) ; and

$d \equiv$ diode gap length (cm) .

J_F should be, in fact, somewhat less than J_{CL} . This difference arises due to the fact that J_{CL} is not derived for the case of a pure field emission mechanism. Rather, there must be an ample supply of electrons (eg., in the case of electrons emitted from a

heated filament) always available for emission. In the derivation of J_{CL} , one of the boundary conditions is that the electric field at the cathode go to zero due to the presence of the space charge (see [Refs. 4,6,7]). If this were to happen to a pure field emitter, then J would go to zero, and a steady state would not develop. Since the field emitter cannot emit at J_{CL} for any appreciable length of time without shutting itself off, its steady state emission value must be something less:

$$J_F < J_{CL} \quad (\text{pure field emission}) \quad . \quad (4)$$

E. EXPLOSIVE MODEL CURRENT DENSITY REQUIREMENT

It has been shown by Schwirzke [Ref. 2] that, for stainless steel, a current density of $J_E \approx 10^9 \text{ A/cm}^2$ would be required to explode a whisker on the cathode surface in a few (<10) ns by joule heating. Thus, a whisker would need to emit a $J_{avg} = J_E$ for approximately 10 ns before exploding. If the transient oscillation period is small compared to 10 ns, then $J_{avg} \approx J_F$, and

$$J_F \geq J_E \quad (\text{explosive emission}) \quad (5)$$

is required for the explosive emission model. This project will attempt to show that, for a wide range of applied potentials, work functions, and enhancement factors, Eq. (5) cannot be satisfied, thus proving that field emission alone is not capable of providing the current density required by the explosive model.

III. SIMULATION

A. BACKGROUND

The type of simulation model used here is, as [Ref. 8] so aptly puts it, one of the "simplest" possible, viable since the first digital computers came into use in the 1950's. While almost primitive in comparison to the latest innovations in so-called "particle-in-cell" simulations [Ref. 8], the model used here nevertheless is time-tested and has worked quite well for the rather simple events under investigation. Although the basic techniques are over three and a half decades old, the actual program is original and is included (in one form) in Appendix B for scrutiny. The program is written in the "C" language and was run on a Sun SPARCstation 2 incorporated into a system running SunOS™ 4.1.1..

B. SIMULATION THEORY

In general terms, the simulation works as follows. Space charge is simulated not as a continuous beam of electrons, but rather as a series of infinitely thin, numerous charged disks of varying charge density σ [C/m²]. In each time interval, the forces on the disks within the gap are computed, the disks are moved, and a new disk is created at the cathode. When a disk reaches the anode, it is no longer used in any further calculations. In the final steady state, all of the disks will have the same charge density; for every time step just as much charge is lost at the anode as is created at the cathode.

1. Electric Field

The charge density σ is calculated by multiplying the time step Δt by the current density J (Eq. 2)⁶

$$\sigma = -J \Delta t . \quad (6)$$

The field-emitted current density at the cathode surface depends on $E_{sc}(0)$, the value of the electric field at the cathode due to all of the space charge disks, and E_{app} , the component of the electric field at the cathode surface due to the applied potential across the diode. In order to find $E_{sc}(0)$, one starts with the one-dimensional Poisson's Equation [Ref. 6]

$$\frac{d^2 V(x)}{dx^2} = \frac{q(n_i - n_e)}{\epsilon_0} , \quad (7)$$

which, for the ion density $n_i = 0$ and the electron charge $q = -e$ becomes

$$\frac{d^2 V(x)}{dx^2} = \frac{e n(x)}{\epsilon_0} , \quad (8)$$

where

$V \equiv$ potential (V) ;

$x \equiv$ position (= 0 at cathode, = d at anode) (m) ;

$e \equiv$ | electron charge | = 1.60×10^{-19} C ;

$n \equiv$ electron number density (m^{-3}) ; and

$\epsilon_0 \equiv$ permittivity of free space = 8.85×10^{-12} C²/N-m² .

⁶ The current density J will always be defined as positive, hence a negative sign has been added on the right side of Eq. (6).

Using $dV(x)/dx = -E(x)$, one gets

$$\frac{dE(x)}{dx} = \frac{-e n(x)}{\epsilon_0} . \quad (9)$$

Integrating both sides over the gap, using the relation $E_{sc}(d) = -E_{sc}(0)$, and rearranging yields

$$E_{sc}(0) = \frac{1}{2\epsilon_0} \int_0^d e n(x) dx . \quad (10)$$

Now, using the charged disk concept, the integral becomes a summation

$$E_{sc}(0) = \frac{1}{2\epsilon_0} \sum_{gap} e n_k \Delta x . \quad (11)$$

where $n_k \equiv$ electron number density [m^{-3}] in disk number k . Realizing that $e n \Delta x = -\sigma$ yields

$$E_{sc}(0) = \frac{1}{2\epsilon_0} \sum_{gap} -\sigma_k . \quad (12)$$

Finally, using Eq. (6),

$$E_{sc}(0) = \frac{1}{2\epsilon_0} \sum_{gap} J_k \Delta t . \quad (13)$$

For a disk located at a point x' in the gap, $E_{sc}(x')$ can be determined from Eqs. (9) and (10) by breaking the integral of the left-hand-side into two parts and subtracting:

$$\int_{E_{sc}(0)}^{E_{sc}(x')} dE_{sc}(x) = \frac{1}{\epsilon_0} \int_0^{x'} -e n(x) dx \quad (14a)$$

becomes

$$E_{sc}(x') - E_{sc}(0) = -\frac{1}{\epsilon_0} \sum_{0 \rightarrow x'} J_k \Delta t , \quad (14b)$$

and

$$\int_{E_{sc}(x')}^{E_{sc}(d)} dE_{sc}(x) = \frac{1}{\epsilon_0} \int_{x'}^d -e n(x) dx \quad (15a)$$

becomes

$$E_{sc}(d) - E_{sc}(x') = -\frac{1}{\epsilon_0} \sum_{x' \rightarrow d} J_k \Delta t . \quad (15b)$$

Subtracting Eq. (15b) from Eq. (14b) and rearranging yields

$$E_{sc}(x') = \frac{1}{2\epsilon_0} \sum_{x' \rightarrow d} J_k \Delta t - \frac{1}{2\epsilon_0} \sum_{0 \rightarrow x'} J_k \Delta t . \quad (16)$$

Eq. (16) is equivalent to saying that the space charge "in front" ($x' \rightarrow d$) will contribute positively to the electric field at x' , whereas the space charge "behind" ($0 \rightarrow x'$) will contribute negatively.

If the applied voltage remains constant, so will the applied electric field E_{app} . The total electric field at x' is therefore⁷

$$E_T(x') = -E_{app} + \frac{1}{2\epsilon_0} \sum_{x' \rightarrow d} J_k \Delta t - \frac{1}{2\epsilon_0} \sum_{0 \rightarrow x'} J_k \Delta t . \quad (17)$$

At the cathode, the enhancement factor must be included:

$$F = -m E_T(0) = m \left\{ E_{app} - \frac{1}{2\epsilon_0} \sum_{gap} J_k \Delta t \right\} . \quad (18)$$

A schematic diagram of the electric field components in the diode is shown in Fig. 6.

⁷ Like F , E_{app} will be defined as a positive quantity, so the appropriate sign change must be made.

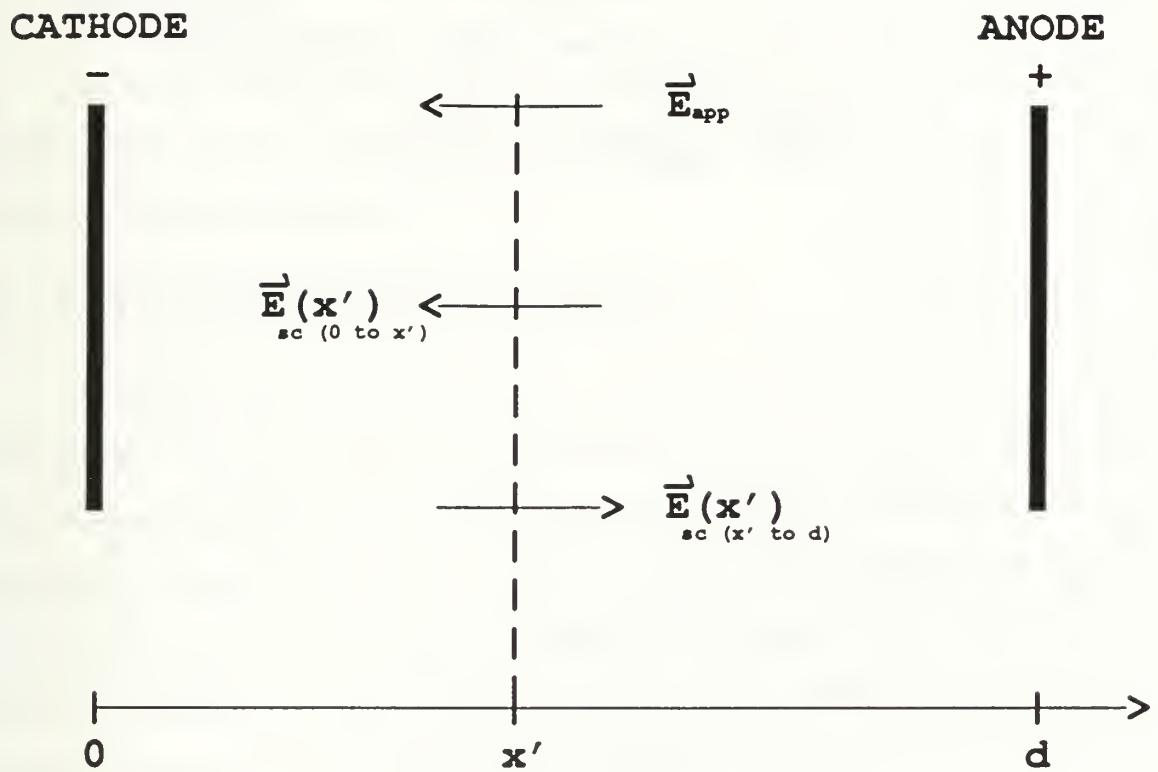


Figure 6. Schematic diagram of electric field components in diode.

2. Equation Of Motion

The nature of the large ($\geq 10^6$ V) applied potentials used in the simulation requires that relativistic equations of motion be used. For any electron in a disk at a position x , the relation is (based on mass \times acceleration = charge \times E-field)

$$\frac{d(\gamma\vec{\beta})}{dt} = \frac{q}{Mc} \vec{E}_T(x) = \frac{-e}{Mc} \vec{E}_T(x) , \quad (19)$$

where

$$\gamma \equiv 1 / \sqrt{1 - v^2 / c^2} ;$$

$$\vec{\beta} \equiv \vec{v} / c ;$$

$$t \equiv \text{time (s)} ;$$

$$e \equiv |\text{electron charge}| = 1.6 \times 10^{-19} \text{ C} ;$$

$$M \equiv \text{electron mass} = 9.11 \times 10^{-31} \text{ kg} ;$$

$$c \equiv \text{speed of light in vacuum} = 3.0 \times 10^8 \text{ m/s} ;$$

$$\vec{E}_T(x) \equiv \text{total electric field at position } x \text{ (V/m)} ;$$

$$x \equiv \text{position (} = 0 \text{ at cathode, } = d \text{ at anode) (m)} ; \text{ and}$$

$$\vec{v} \equiv \text{velocity (m/s)} .$$

Substituting into Eq. (19) and carrying out the derivative gives

$$\vec{v} \frac{d\gamma}{dt} + \gamma \frac{d\vec{v}}{dt} = \frac{-e}{M} \vec{E}_T(x) . \quad (20)$$

Taking the derivative of γ and substituting in yields

$$(\beta^2 \gamma^3 + \gamma) \frac{d\vec{v}}{dt} = \frac{-e}{M} \vec{E}_T(x) . \quad (21)$$

With a little more substituting, Eq. (21) can be solved for $d\vec{v} / dt$:

$$\frac{d\vec{v}}{dt} = \frac{-e}{M \gamma^3} \vec{E}_T(x) . \quad (22)$$

Eq. (22) is the equation of motion used in the simulation.

IV. RESULTS

A. OBJECTIVE

Again, the goal of the simulations is to show that the value of J_F for a given set of conditions will not be greater than the 10^9 A/cm^2 required by the elementary explosive emission model (Eq. (5)).

B. METHODS OF OBTAINING RESULTS

For lesser values ($< 10^6 \text{ A/cm}^2$) of J_0 (the value of the current density at the cathode at $t = 0$; i.e., with the potential applied but no space charge in the gap yet) the program is easily capable of running through the transient period and into the final state (as in Fig. 7a) in a short (\approx computer *hours*) period of time. But for larger values of J_0 , the run time goes up considerably (\approx computer *days*). The objective requires only that $J_F < J_E$ is proven; it is possible to do this without running the program through to the final state by using three simple "tricks":

1. Attempt to simulate the steady-state electric field at the cathode by artificially adding in, at $t = 0$, an estimate of the steady-state space charge. The artificial charge will be an immovable source located at the anode so that it will always be "in front" of the emitted charges;
2. Remove equal parts of the artificial space charge during each time step of the simulation, until it is all removed; and
3. Set the amount of artificial space charge removed each time step equal to the amount created at the cathode in the first time step.

Although the resulting plots will certainly be non-physical (no such artificial space charge exists in reality), the graphical output can nonetheless be definitively interpreted.

During the early phase of the removal period, the graph of J vs. t will be a horizontal straight line, as in the final steady state (just as much space charge is removed each period as is put in, so J will not change) (see Figs. 7b,c,d). If the estimate of the steady-state space charge is exactly correct, the graph of J vs. t will continue to be straight, even after all of the artificial space charge is removed, because in this case the simulation will have started equivalent to the steady state. Thus, if the graph remains flat after all the artificial space charge is gone, the value of J_F will be known exactly (see Fig. 7b). Guessing the exact value of the steady state space charge is, however, highly unlikely.

If the estimate of the steady-state space charge is too high, the value of F will be smaller than in the actual steady-state case, and the value of J during the early phase of the removal period will be lower than the actual J_F . In this case some of the artificial charge will still exist when the first emitted electrons reach the anode. At this point, the amount of charge lost each time period will increase, thus increasing F and J (see Fig. 7c).

More useful, however, is the case where the estimate of the steady-state space charge is too low. The value of F will be larger than in the actual steady-state case, and J will be larger than the actual J_F . In this case, the artificial charge will be used up before the first emitted electrons reach the anode. Once all of the artificial charge is gone, the value of F will drop as more charge enters the gap while none is removed (see Fig. 7d). It can be concluded that the early removal phase value of J is greater than the actual J_F . An upper bound on J_F can thus be found by this "maximum value method", and if the calculated upper bound is less than J_E , the objective will have been met.

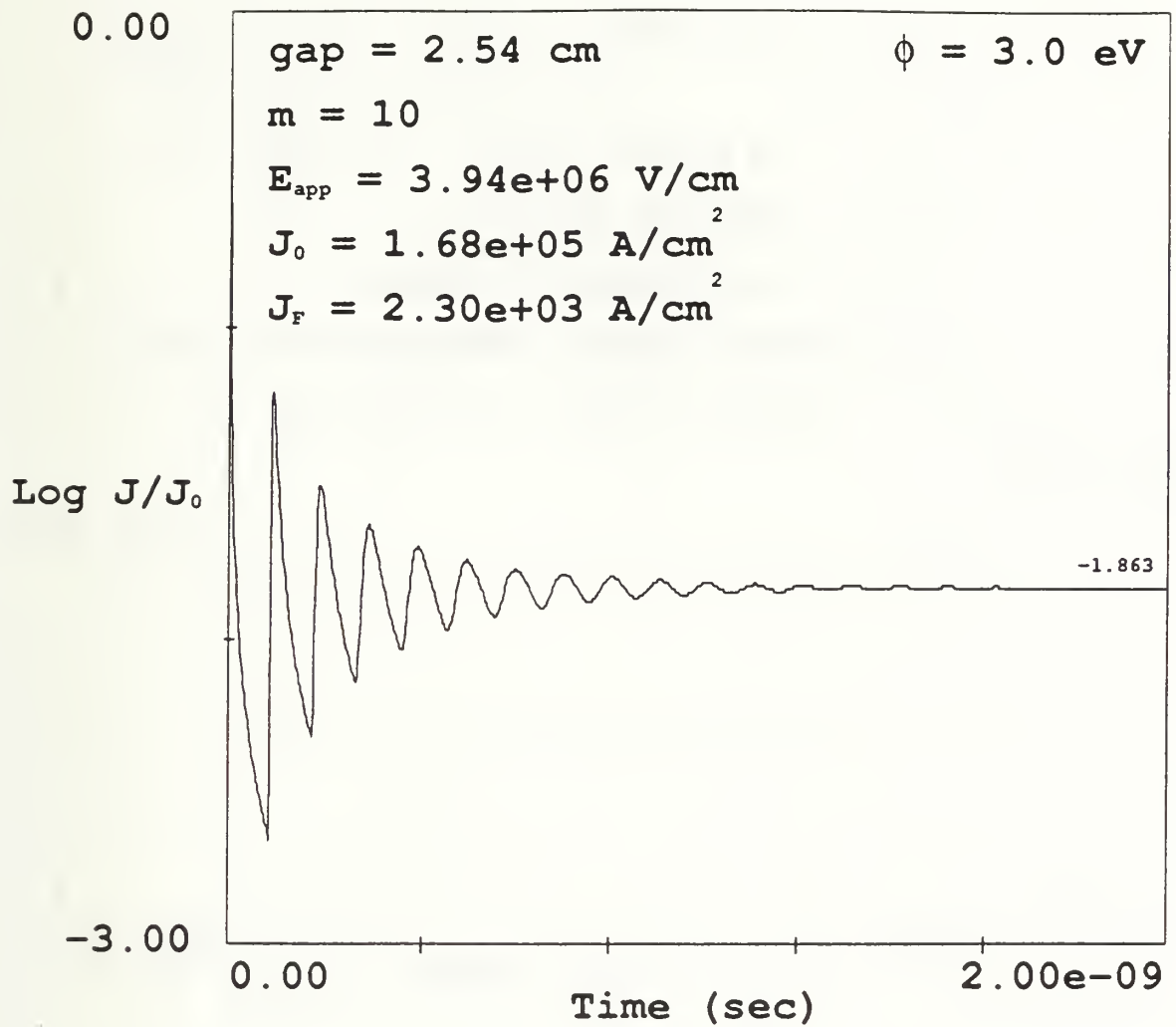


Figure 7a. Log of the current density ratio vs. time. No artificial space charge is added, and the simulation is run until the final steady state is reached (2 ns). The steady-state ratio is $J/J_0 = 1.37 \times 10^{-2}$.

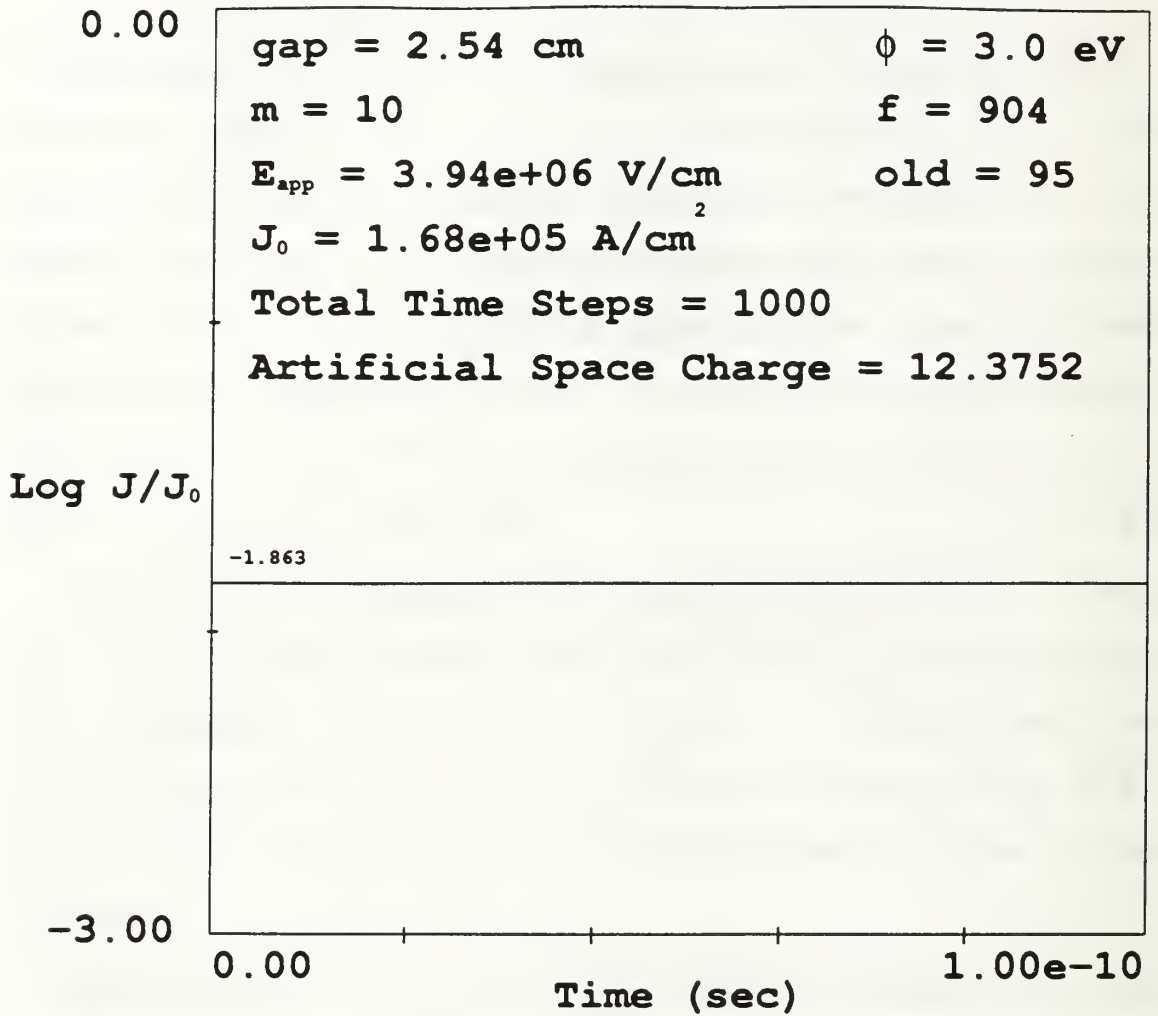


Figure 7b. Log of the current density ratio vs. time. Enough artificial space charge was added to simulate the steady state of Fig. 7a exactly (12.3752 dimensionless units). The value of f is the number of time steps required to use up the artificial charge. The value of old indicates the time step of creation for the charge disk closest to the anode. If $f > 0$, $old > 1$, and the plot is straight, then the line is at the equilibrium value. Note the run-time is 0.1 ns (1/20 of the full-run time-steps in Fig. 7a).

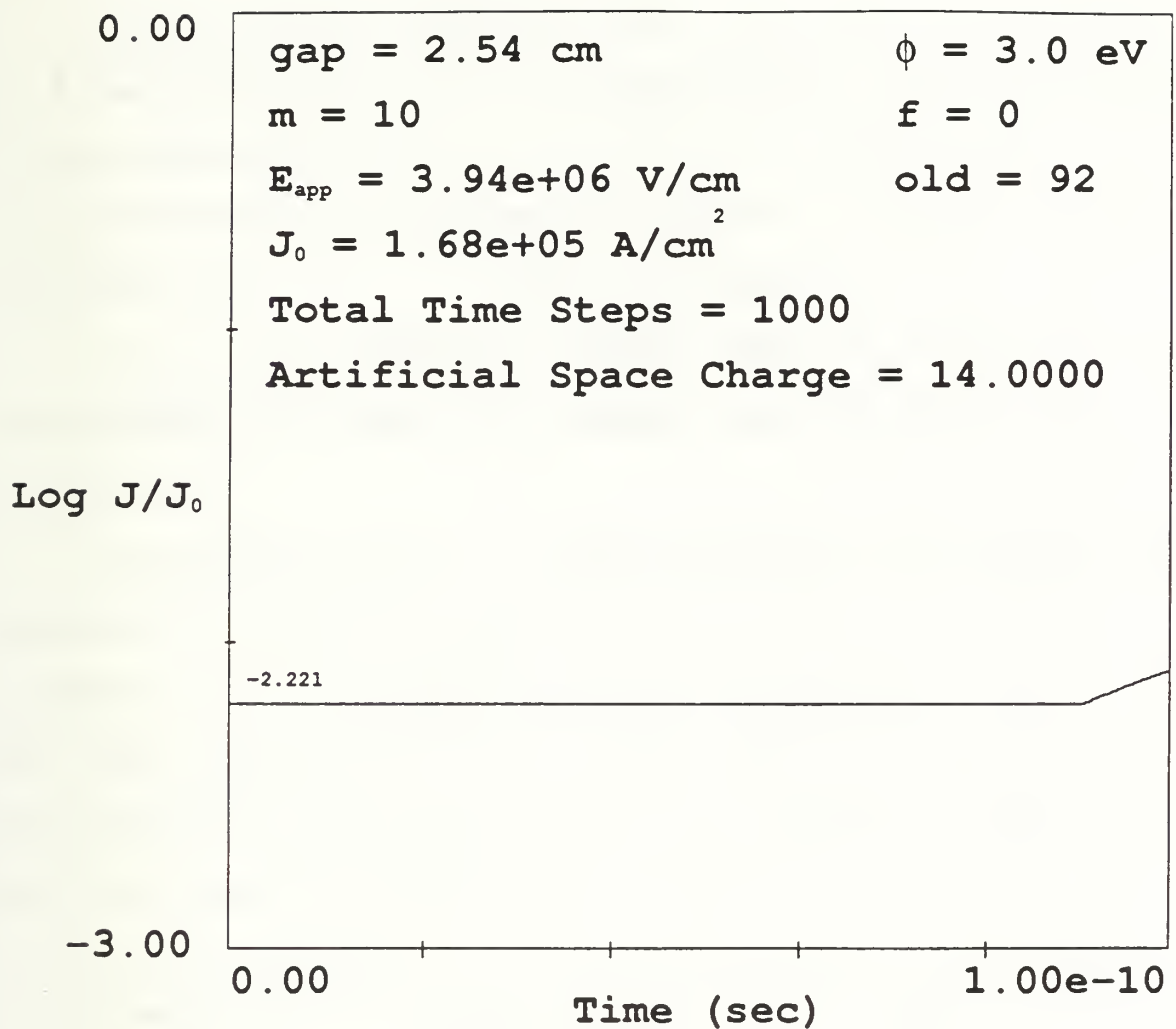


Figure 7c. Log of current density ratio vs. time. More than the equilibrium value of the space charge has been artificially inserted (14 dimensionless units). In this case, $f = 0$, $old > 1$ indicates that the artificial space charge has not been used up before the first disk reached the anode; the plot rises at the end as expected. Again, only 1/20 of the full-run time-steps is required to obtain a result (in this case, a lower bound on J_F).

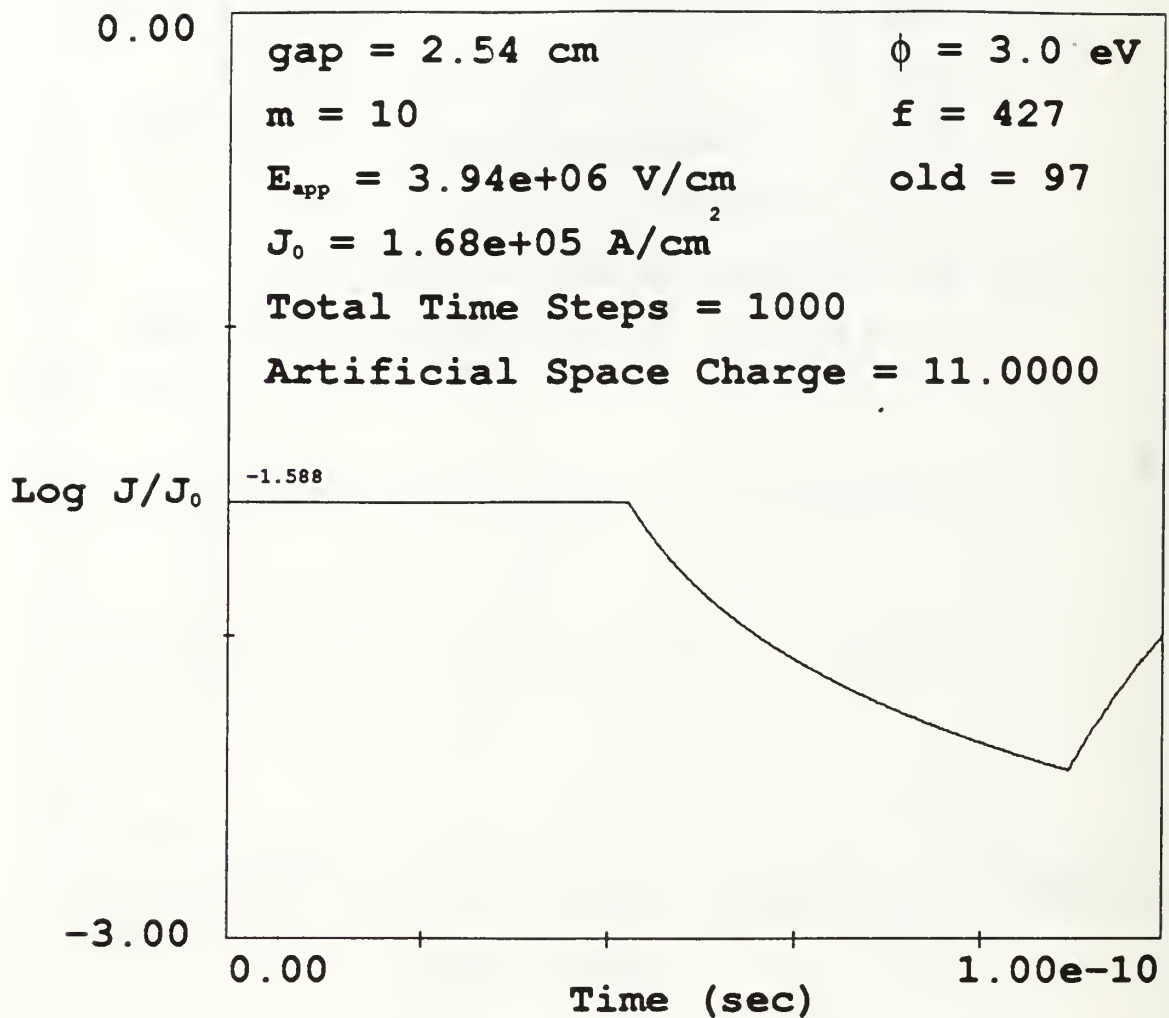


Figure 7d. Log of current density ratio vs. time. Less than the equilibrium value of the space charge has been artificially inserted (11 dimensionless units). In this case, $f > 0$ and $\text{old} > 1$, but the plot drops from the early-phase flat portion. Note that the early phase value (-1.588) is greater than the steady state value (-1.863) of Fig. 7a. An upper bound on the current density has been determined in only 1/20 of the full-run time-steps.

C. SIMULATION RESULTS

As can be seen in the last column of Table 1, under nearly all tested conditions, $J_F < J_E = 10^9 \text{ A/cm}^2$. In fact, in most cases, J_0 was less than J_E , indicating that only for high applied electric fields ($> 3 \times 10^6 \text{ V/cm}$) and large enhancement factors (> 100) would there even be a possibility for the final value of the current density to exceed the explosive limit.

For those cases where it was not shown that $J_F < J_E$ (denoted by ‡), the excessive amount of run time (\approx computer days) to lower the maximum level was just too prohibitive.

It was predicted earlier that J_F would be less than the Child-Langmuir space charge limited current density J_{CL} (Eq. (4)). The program was run long enough (when possible) for the $\phi = 3.0 \text{ eV}$ case to determine if the maximum of J_F is indeed less than J_{CL} . The results are summarized in Table II. Similar results are expected for $\phi = 4.0$ and 5.0 eV as well, since the values of J_0 (and logically the maximum J_F also) are lower for these two cases than for the $\phi = 3.0 \text{ eV}$ case.

TABLE I. SIMULATION RESULTS[†]

E_{app} (V/cm)	ϕ (eV)	m	J_0 (A/cm ²)	J_F (A/cm ²)
3.94×10^5	5.0	1	≈ 0	≈ 0
3.94×10^5	5.0	10	≈ 0	≈ 0
3.94×10^5	5.0	100	5.86	4.93
3.94×10^5	5.0	300	9.92×10^6	$\leq 7.84 \times 10^6$ *
3.94×10^5	4.0	1	≈ 0	≈ 0
3.94×10^5	4.0	10	≈ 0	≈ 0
3.94×10^5	4.0	100	1.30×10^3	8.69×10^1
3.94×10^5	4.0	300	6.98×10^7	$\leq 6.97 \times 10^7$ *
3.94×10^5	3.0	1	≈ 0	≈ 0
3.94×10^5	3.0	10	≈ 0	≈ 0
3.94×10^5	3.0	100	1.68×10^5	2.17×10^2
3.94×10^5	3.0	300	4.27×10^8	$\leq 5.00 \times 10^5$ *
3.94×10^6	5.0	1	≈ 0	≈ 0
3.94×10^6	5.0	10	5.86	5.77
3.94×10^6	5.0	100	7.73×10^9	$\leq 6.81 \times 10^7$ *
3.94×10^6	5.0	300	2.34×10^{11}	$\leq 4.24 \times 10^7$ *
3.94×10^6	4.0	1	≈ 0	≈ 0
3.94×10^6	4.0	10	1.30×10^3	4.84×10^2
3.94×10^6	4.0	100	1.62×10^{10}	$\leq 7.24 \times 10^7$ *
3.94×10^6	4.0	300	3.48×10^{11}	$\leq 7.39 \times 10^7$ *
3.94×10^6	3.0	1	≈ 0	≈ 0
3.94×10^6	3.0	10	1.68×10^5	2.30×10^3
3.94×10^6	3.0	100	3.42×10^{10}	$\leq 8.00 \times 10^6$ *
3.94×10^6	3.0	300	5.41×10^{11}	$\leq 9.00 \times 10^6$ *
3.94×10^7	5.0	1	5.86	5.85
3.94×10^7	5.0	10	7.73×10^9	$\leq 6.81 \times 10^7$ *
3.94×10^7	5.0	100	3.98×10^{12}	$\leq 8.00 \times 10^8$ *
3.94×10^7	5.0	300	4.05×10^{13}	$\leq 7.00 \times 10^9$ ‡ *
3.94×10^7	4.0	1	1.30×10^3	1.07×10^3
3.94×10^7	4.0	10	1.62×10^{10}	$\leq 7.24 \times 10^7$ *
3.94×10^7	4.0	100	5.25×10^{12}	$\leq 8.00 \times 10^8$ *
3.94×10^7	4.0	300	5.15×10^{13}	$\leq 7.00 \times 10^9$ ‡ *
3.94×10^7	3.0	1	1.68×10^5	1.55×10^4
3.94×10^7	3.0	10	3.42×10^{10}	$\leq 8.00 \times 10^6$ *
3.94×10^7	3.0	100	7.32×10^{12}	$\leq 8.01 \times 10^8$ *
3.94×10^7	3.0	300	6.97×10^{13}	$\leq 7.00 \times 10^9$ ‡ *

[†] For a diode with plate spacing of 1 in = 2.54 cm.

* Indicates maximum value method result.

‡ Indicates run-time-constrained result.

TABLE II.
SIMULATION RESULTS VS. CHILD-LANGMUIR LAW[†]

ϕ (eV)	m	E_{app} (V/cm)	J_{CL} (A/cm ²)	J_0 (A/cm ²)	maximum J_F (A/cm ²)
3.0	1	3.94×10^7	3.62×10^5	1.68×10^5	1.55×10^4
3.0	10	3.94×10^6	1.14×10^4	1.68×10^5	2.30×10^3
3.0	10	3.94×10^7	3.62×10^5	3.42×10^{10}	$8.00 \times 10^6 \ddagger$
3.0	100	3.94×10^5	3.62×10^2	1.68×10^5	2.17×10^2
3.0	100	3.94×10^6	1.14×10^4	3.42×10^{10}	$8.00 \times 10^6 \ddagger$
3.0	100	3.94×10^7	3.62×10^5	7.32×10^{12}	$8.01 \times 10^8 \ddagger$
3.0	300	3.94×10^5	3.62×10^2	4.27×10^8	$5.00 \times 10^5 \ddagger$
3.0	300	3.94×10^6	1.14×10^4	5.41×10^{11}	$9.00 \times 10^6 \ddagger$
3.0	300	3.94×10^7	3.62×10^5	6.97×10^{13}	$7.00 \times 10^9 \ddagger$

D. OTHER GRAPHICAL OUTPUT

The plot of Fig. 7a appears to agree with the basic theory that the value of the emitted current density will oscillate at first, then settle down until a final steady state is reached. But earlier versions of the program encountered problems. In an effort to determine the causes of the difficulties, the program was altered to produce plots of other variables. Figs. 8-11 are some examples run for the same conditions. Although the applied electric field is rather high in these plots, the results are nonetheless representative of the output for the applicable range of electric fields. Short computer running time was the primary factor in the choice of parameters for these examples.

[†] For a diode with plate spacing of 1 in = 2.54 cm.

[‡] Indicates run-time-constrained result.

Fig. 8a shows how the velocity of the disks varies with distance. This plot shows that the need for relativistic equations of motion is quite real. Fig. 8b is a blow-up of Fig. 8a which shows that the velocity reaches 2.98×10^{10} cm/s by the time a disk gets only 5 % of the way across the gap.

Fig. 9a shows how the density, similar to the velocity, is nearly constant across the gap (at equilibrium). This is to be expected at equilibrium, as all of the disks have the same charge density and most are moving at essentially the same speed. Fig. 9b is a blow-up of Fig. 9a, showing that the value of the density at 5 % of the way across the gap is within approximately 0.5 % of the value at the anode. The density is greater near the cathode because the slower moving electrons there are still "bunched", whereas those farther away are fully separated by the acceleration process.

If the density is essentially constant, the electric field should appear as a sloping straight line centered about E_{app} . Fig. 10a shows the magnitude of the electric field vs. distance. As predicted, the plot is straight and centered about E_{app} . In order to see the effect of the higher density near the cathode, the plot was blown-up into Fig. 10b. Indeed, a small deviation can be seen near the cathode, as expected.

Running the program over and over again with the same parameters just to get plots of different variables can be time consuming. So three of the plots were combined into one multi-plot. The multi-plot program was then modified to make it into a "cartoon," that is, the plots would update on the screen with each chosen (by the programmer) time step. Fig. 11a shows a multi-plot cartoon freeze-frame at a time just before the current density reached the absolute minimum. As expected, the density plot is high near the anode and low near the cathode. The electric field plot shows

that the E-field at the half-way point across the gap is less than E_{app} , also indicating that there truly is more charge in front of the mid-point than behind it.

In Fig. 11b the time is frozen at a point where the current density has just reached a local maximum. The density graph shows high density at either end of the diode (newly created at the cathode and what's left of the charge at the anode from Fig. 11a). The electric field curve "kinks" in tandem with the new charge in the density plot below it.

Fig. 11c shows the frame in which the current density approaches a local minimum. Note how the density is more spread out than in Fig. 11a, and how there is less curvature to the E-field curve. By Fig. 11d, the next local maximum of the current density has been reached, and by now the density is nearly equal everywhere. The electric field plot is near linearity.

In Fig. 11e the multi-plot is run to the steady-state. The density is constant at all points except near the cathode; the electric field curve is straight and centered about E_{app} , as expected. Based on proper behavior of the above plots, it can be concluded that the simulation program is producing plausible data.

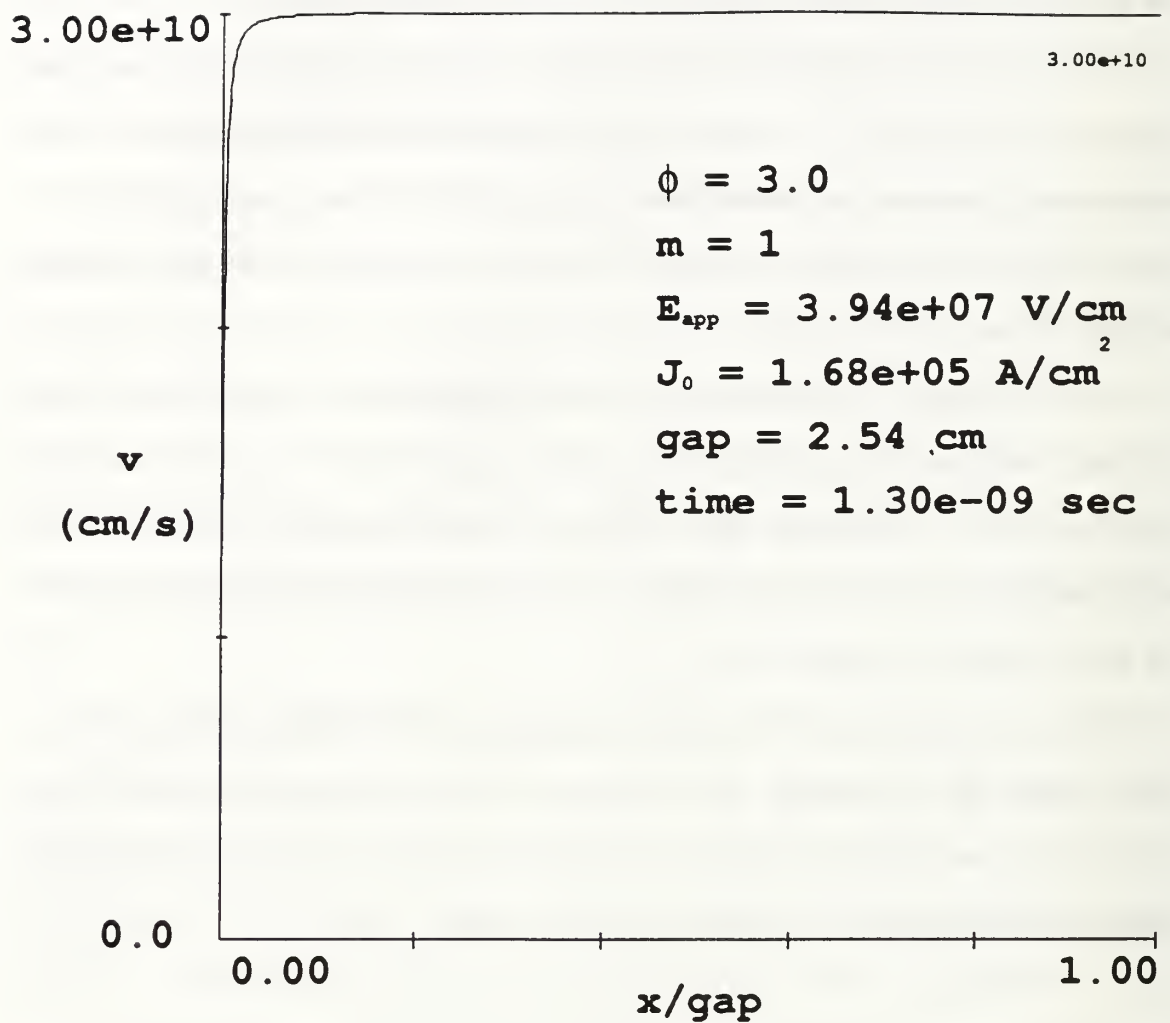


Figure 8a. Space charge velocity vs. distance ratio at equilibrium.

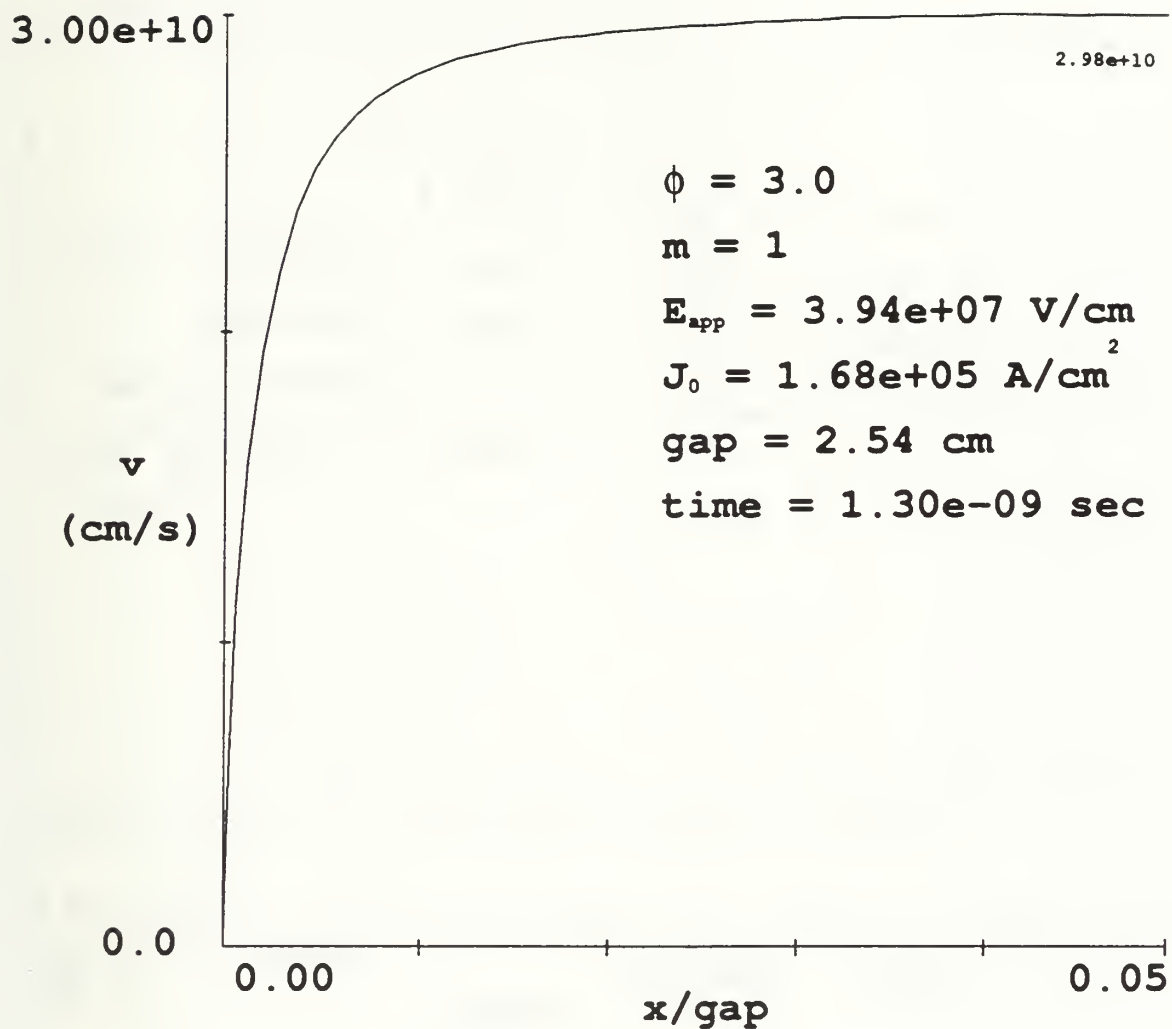


Figure 8b. Space charge velocity vs. distance ratio at equilibrium; first five percent of gap.

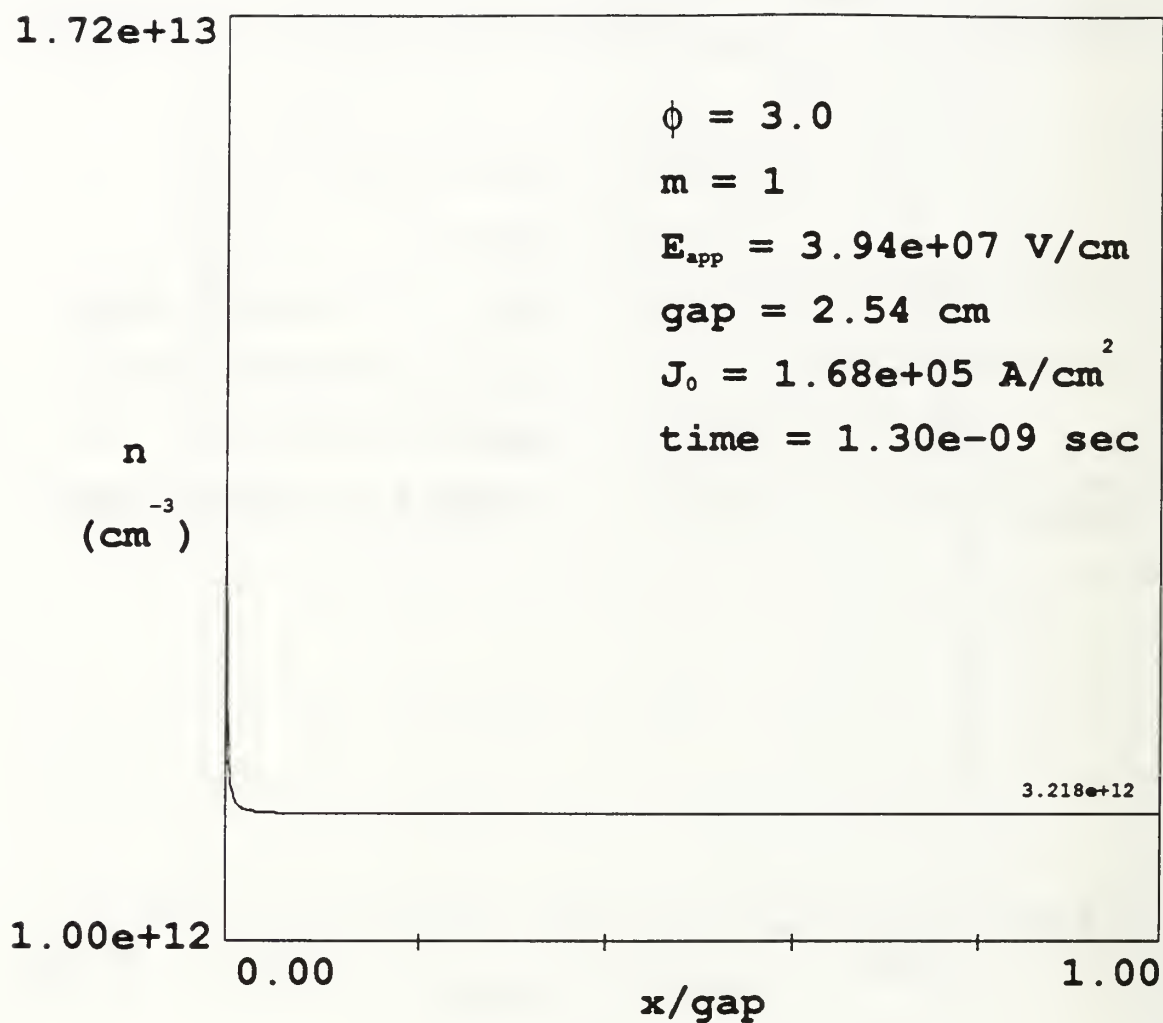


Figure 9a. Space charge density vs. distance ratio at equilibrium.

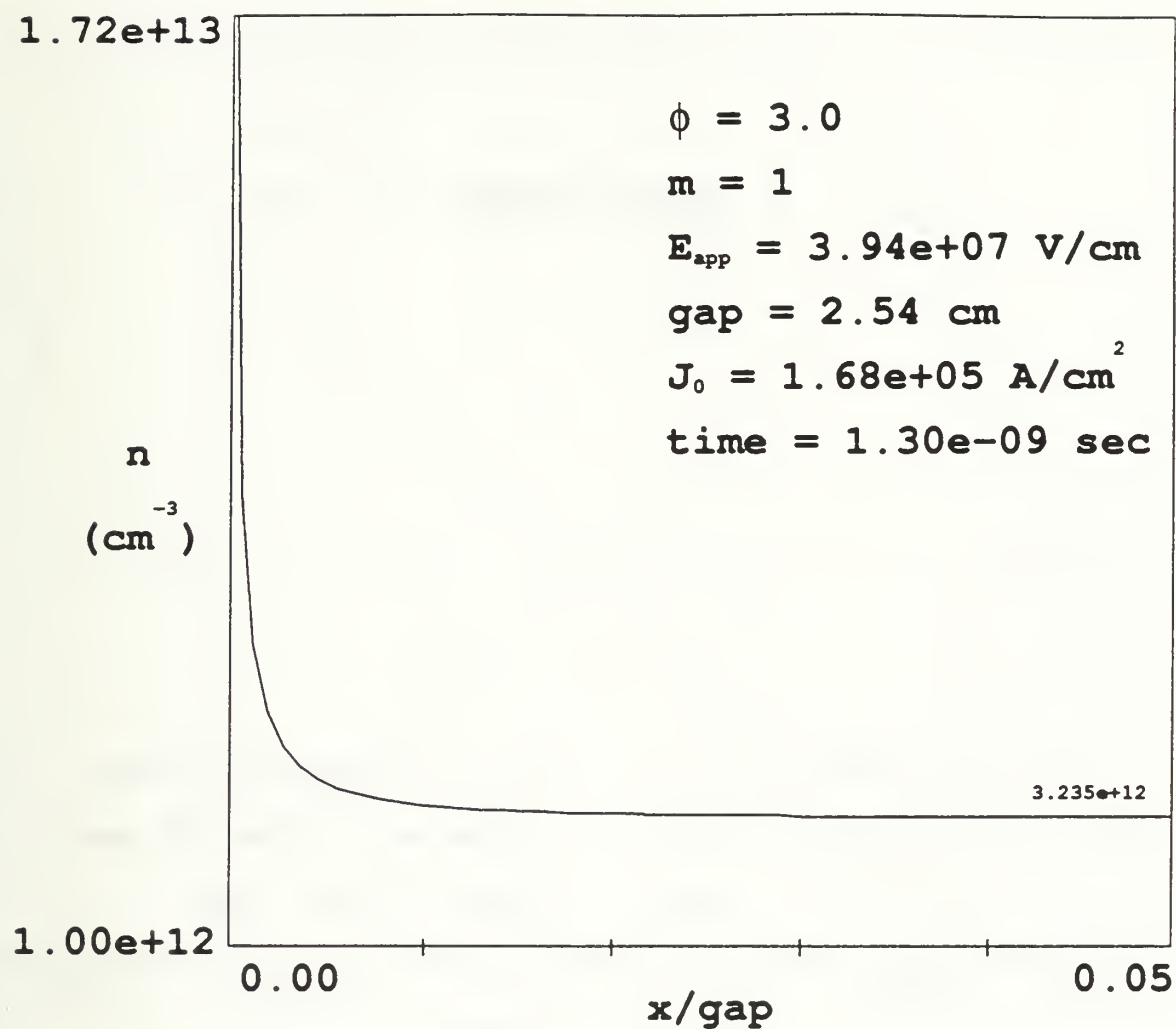


Figure 9b. Space charge density vs. distance ratio at equilibrium; first five percent of gap.

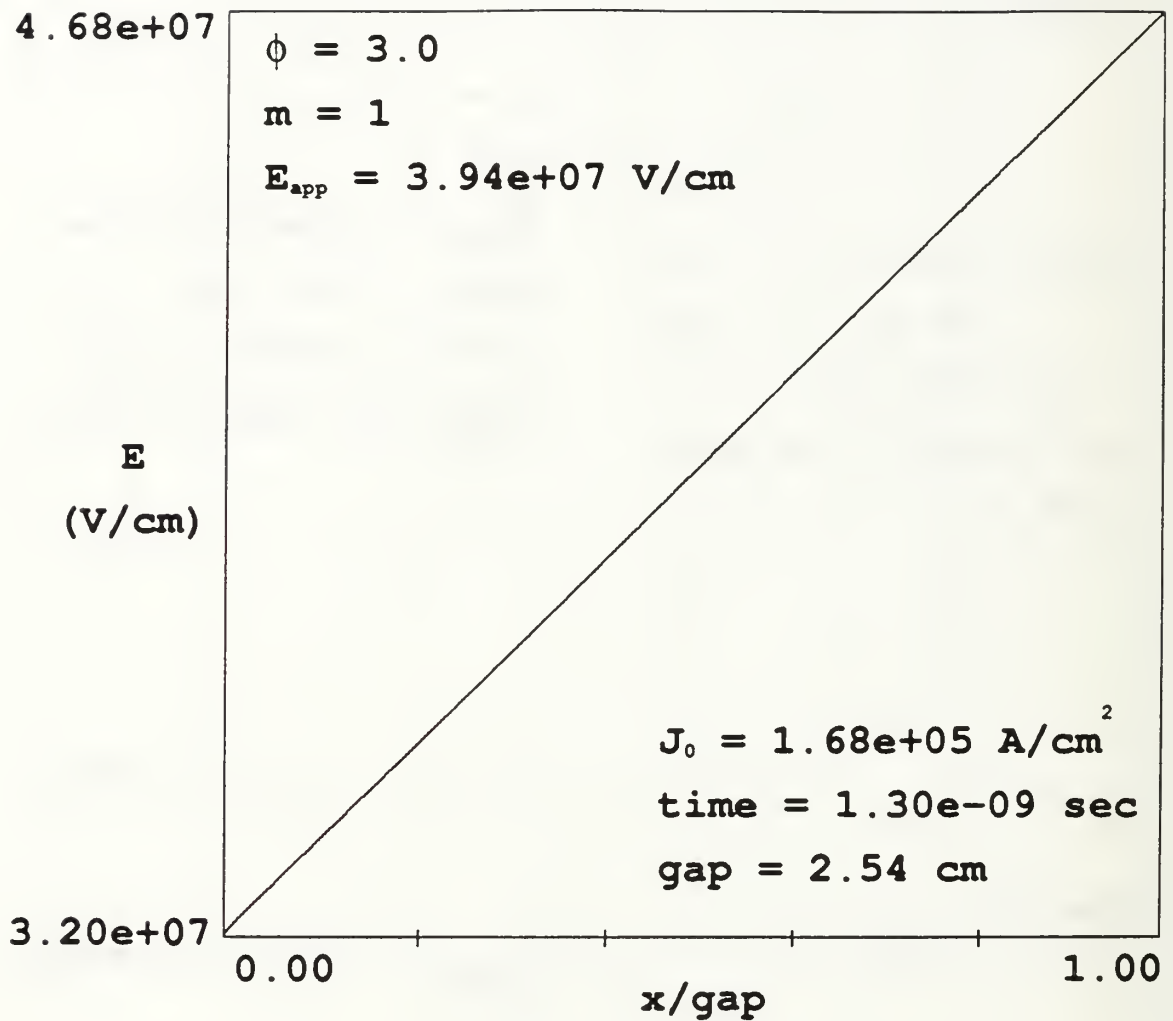


Figure 10a. Electric field vs. distance ratio at equilibrium.

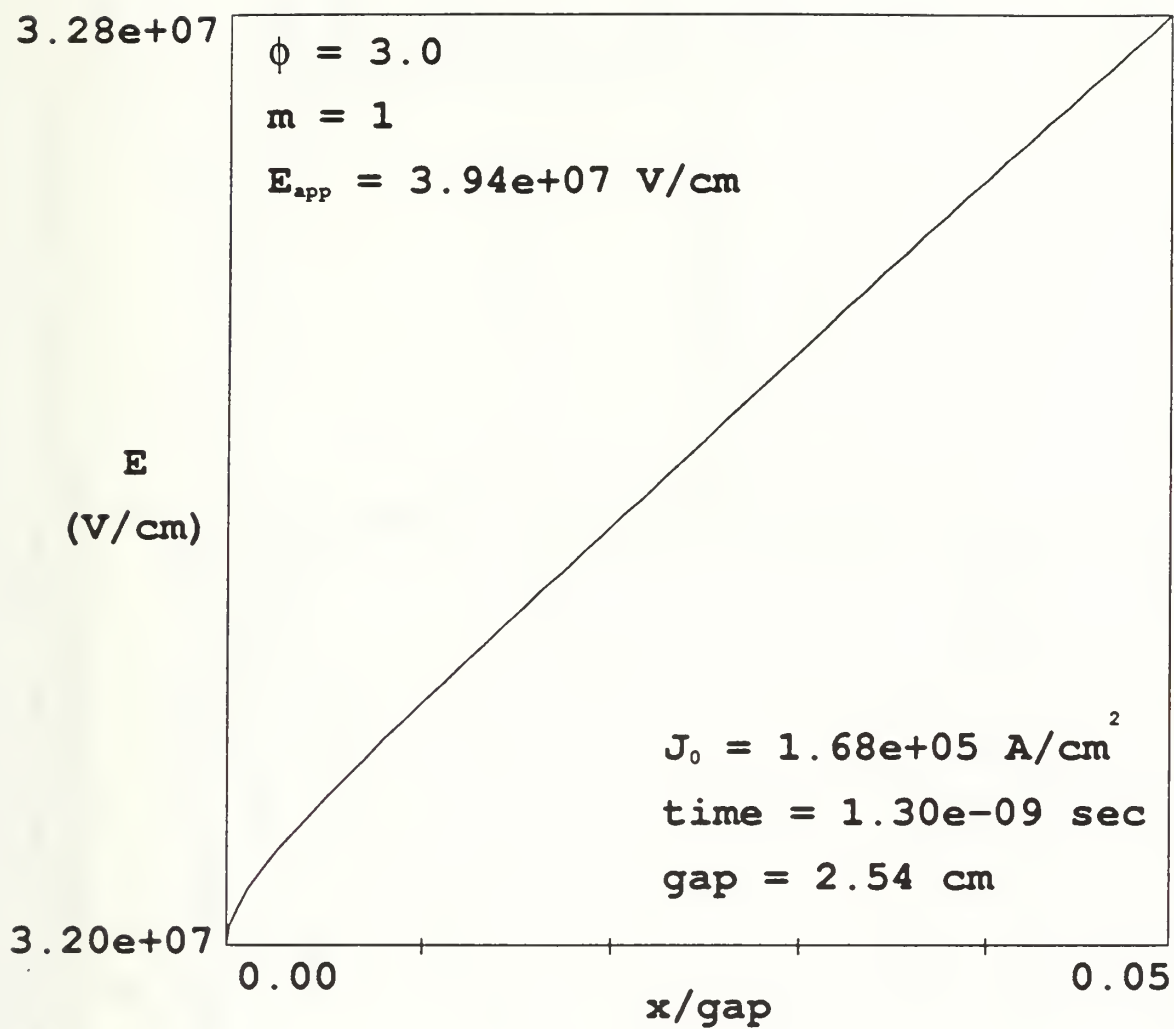


Figure 10b. Electric field vs. distance ratio at equilibrium; first five percent of gap.

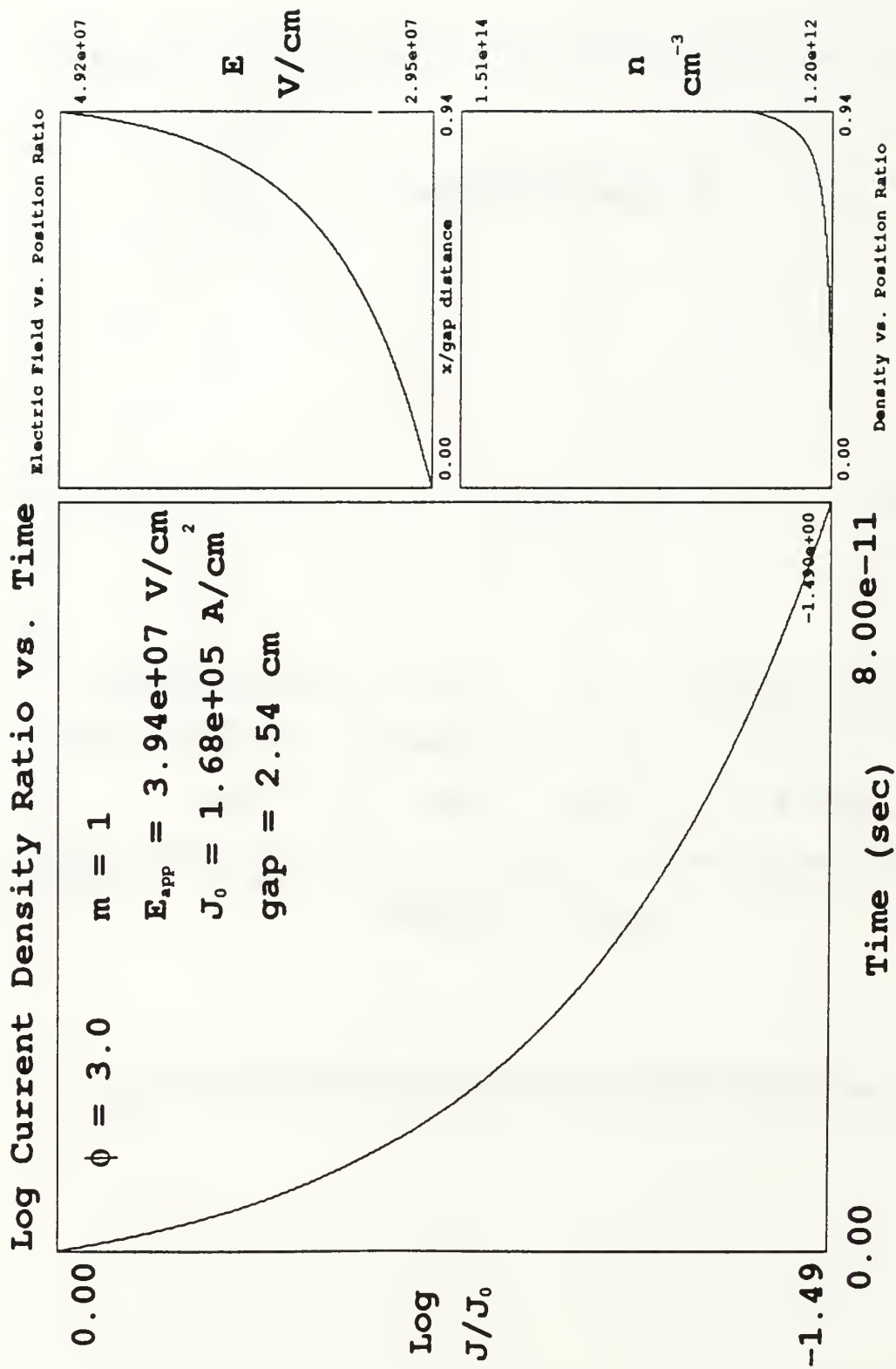


Figure 11a. Multi-plot nearing absolute minimum.

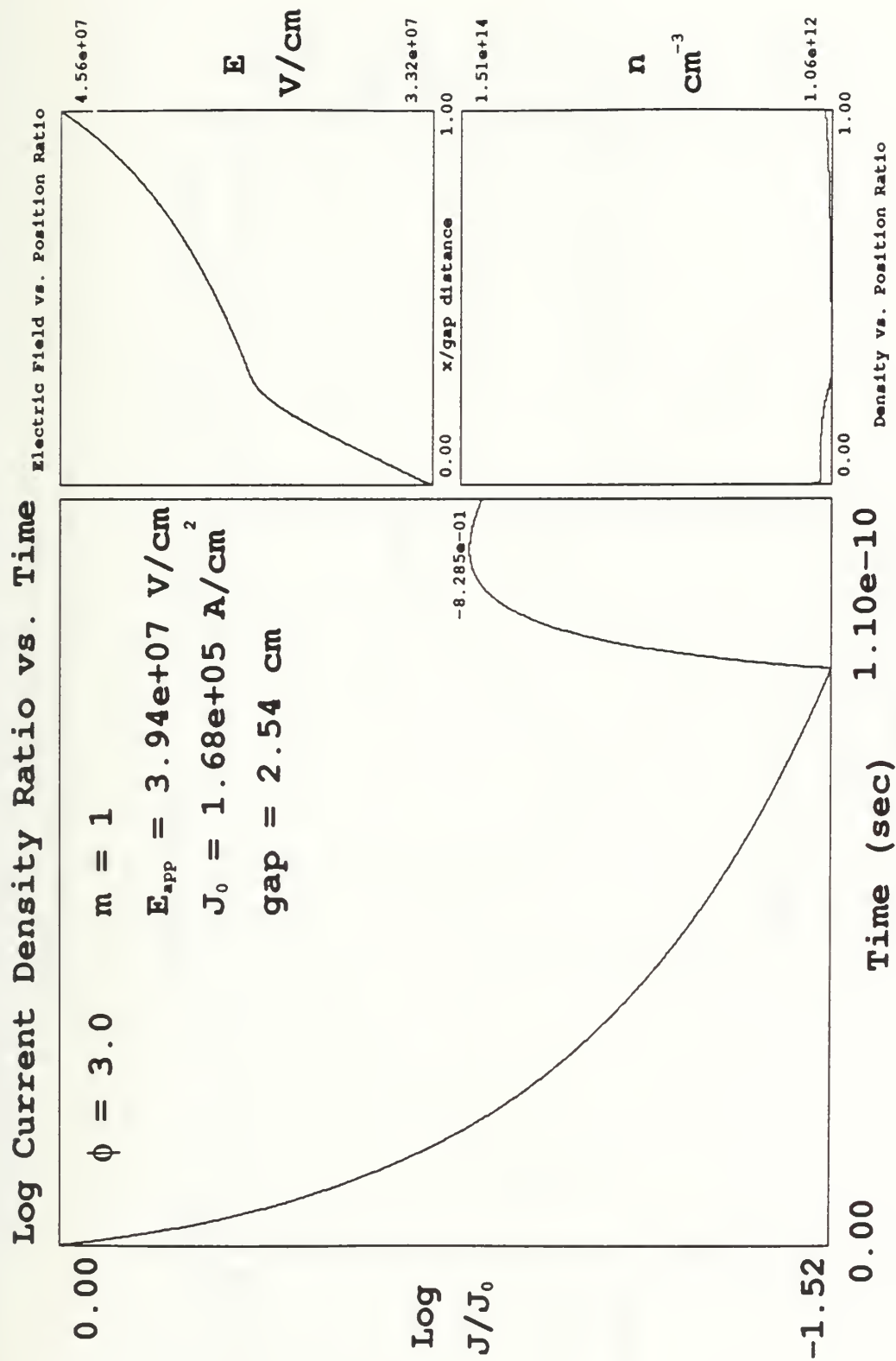


Figure 11b. Multi-plot at first local maximum.

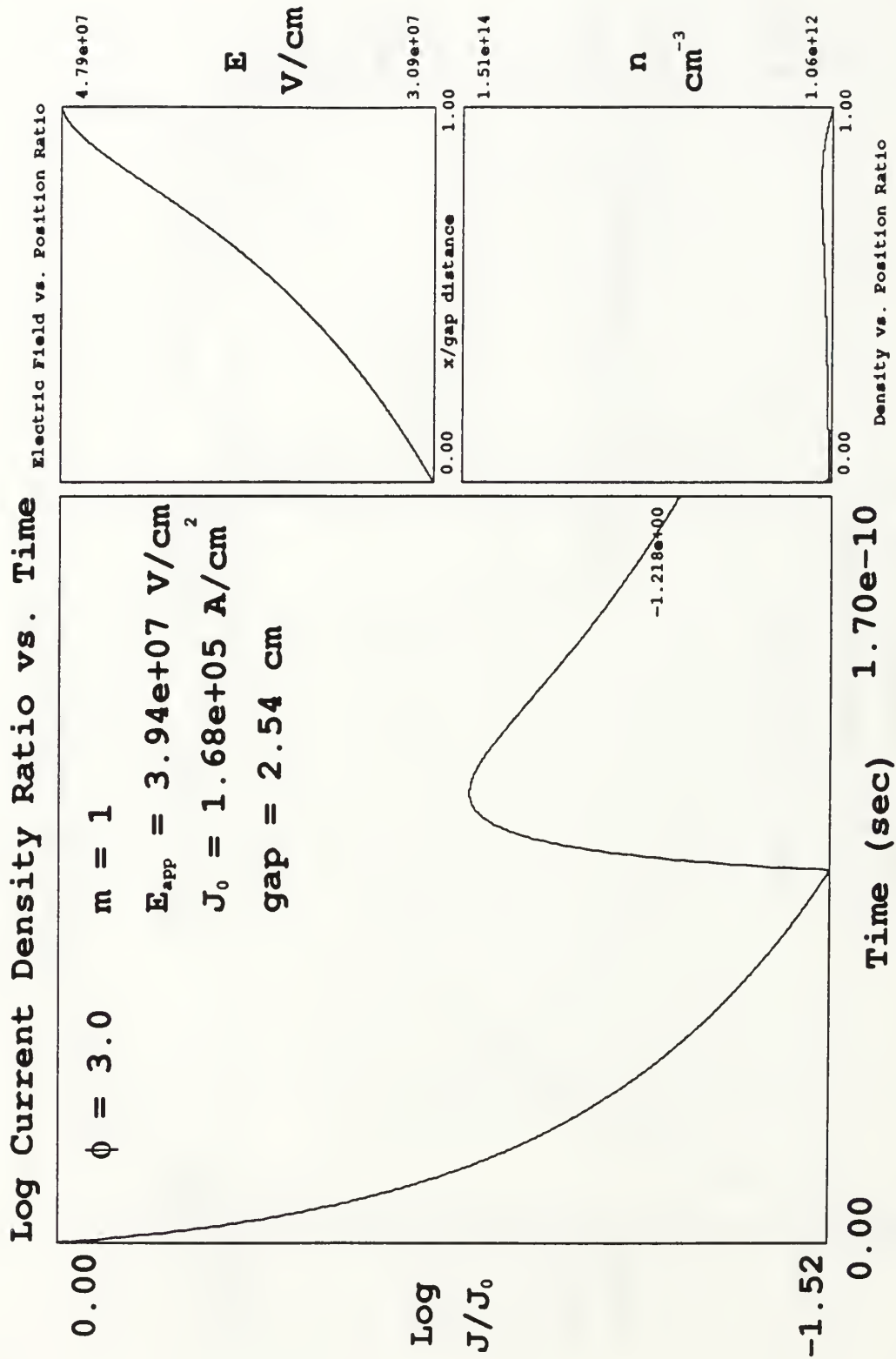
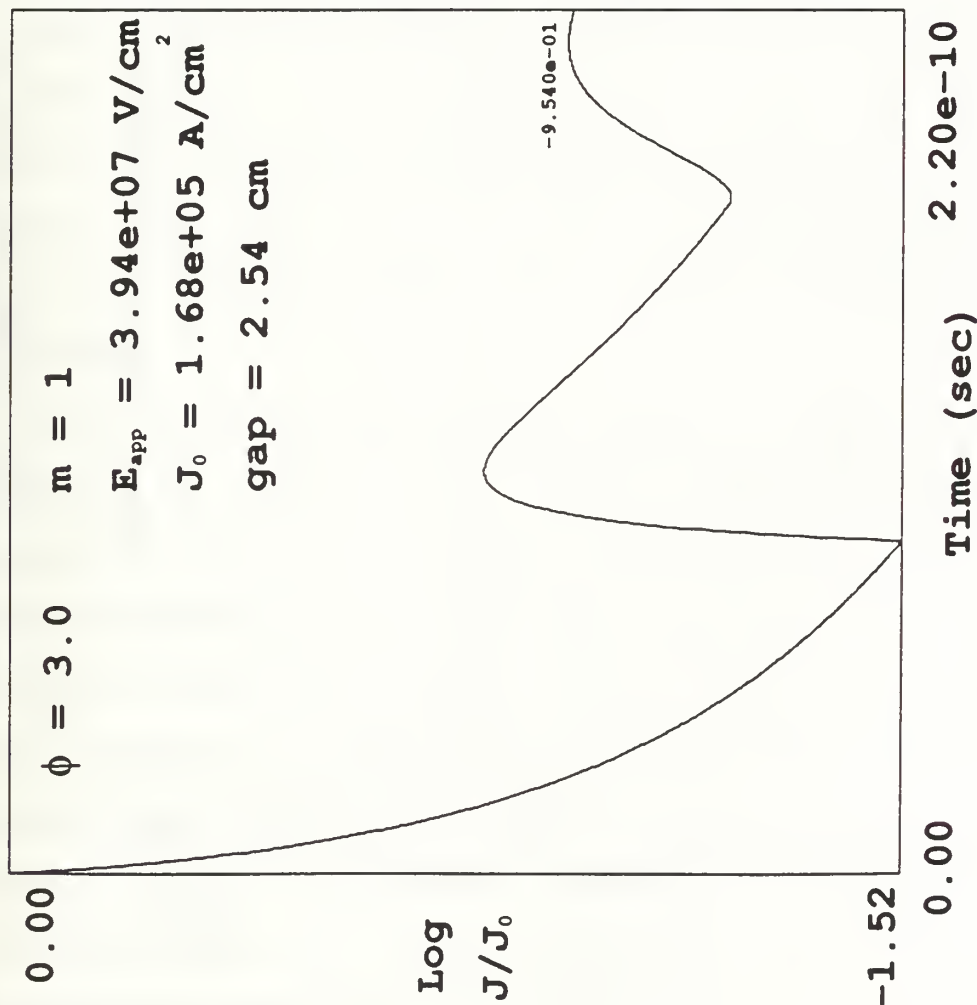


Figure 11c. Multi-plot nearing local minimum.

Log Current Density Ratio vs. Time



Electric Field vs. Position Ratio

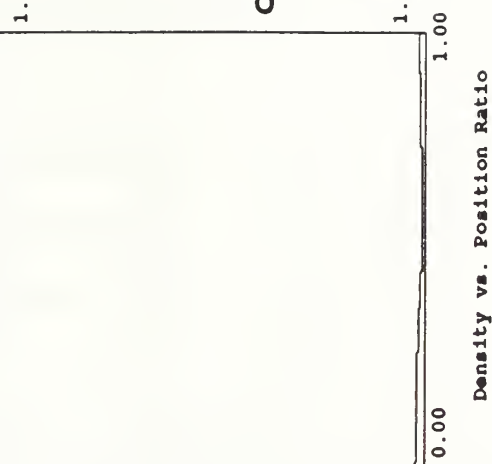
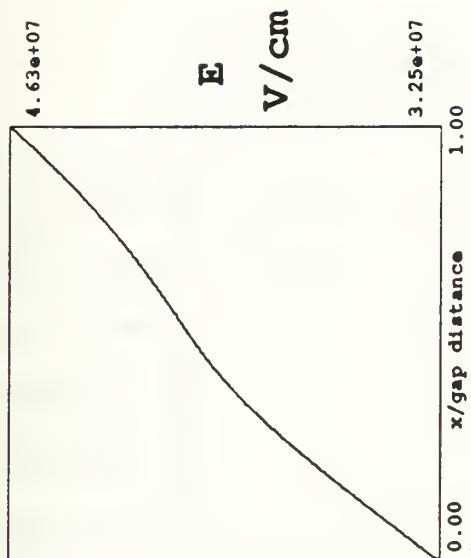
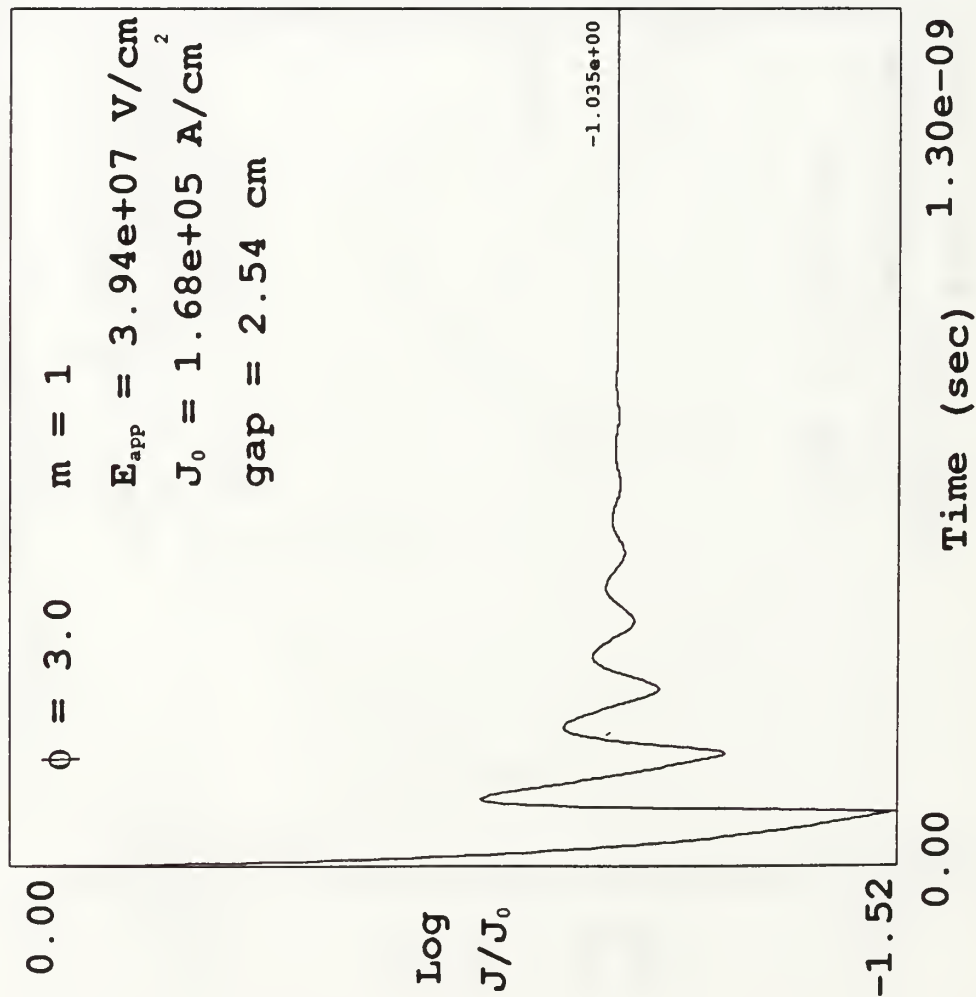


Figure 11d. Multi-plot at second local maximum.

Log Current Density Ratio vs. Time



Electric Field vs. Position Ratio

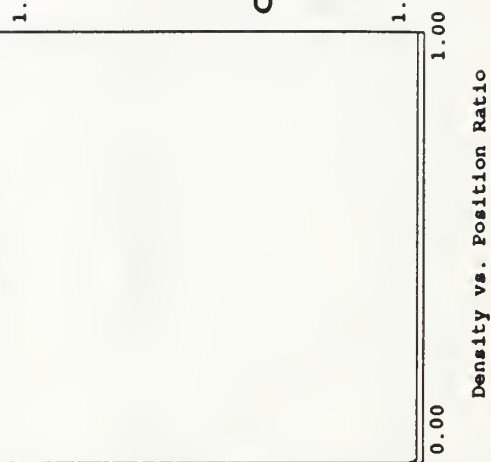
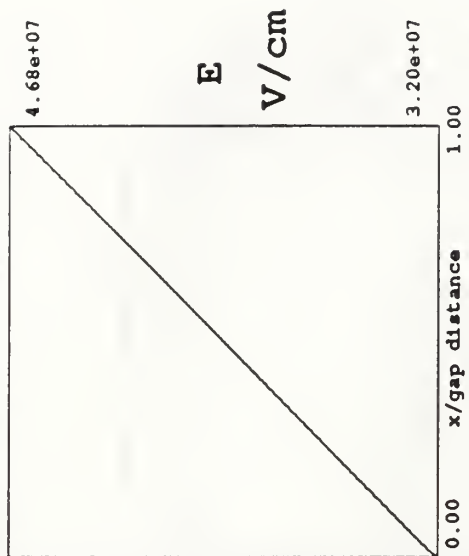


Figure 11e. Multi-plot at equilibrium.

V. CONCLUSIONS

As expected, the final equilibrium value of the current density for a pure field emitter was found to be less than the Child-Langmuir space charge limited current density for the non-run-time-constrained simulations. A comparison of the values is presented in Table II. The run-time-constrained results (denoted by a ‡) cannot be used to either verify or contradict Eq. (4), but based on the arguments of section IID. it is likely that verification would be achieved if longer run-times were feasible.

Based on the simulation results shown in Table I, it can be stated that, except in the cases denoted by a ‡, that $J_F < J_E$. Thus, for a 1 in gap, a purely field-emitted current density is not sufficient to cause the explosion mechanism of a whisker on the cathode to trigger in less than 10 ns. The above noted exceptions may or may not conform to the other data; computer run time constraints did not allow for a definitive determination.

Again, it must be pointed out that this model of only pure field emission is quite elementary in that it does not include the effects of thermionic emission. A whisker certainly heats up due to the emission process and some thermionic emission must be present. In fact, based on the results of those simulations which ran until equilibrium was reached ($mE_{app} \leq 3.94 \times 10^7$ V/cm), it would seem that thermionic emission must be the dominant emission source, at least for those parameters, if the explosive model is truly accurate. Whether enough thermionic emission occurs to validate the explosive model is debatable, especially in cases such as $m = 1$, $E_{app} \leq 3.94 \times 10^6$ V/cm, where the field emission contributes almost nothing to the total emission current density and the applied electric field does not provide much

relative enhancement (compared to higher values of E_{app}) at the metal-vacuum interface. A study done by Hallal [Ref. 3] at such parameters concluded that the explosive model could not account for the breakdown that he observed, and that a Schwirzke-type model seemed more promising. It can be concluded, then, that the explosive model only has a chance of validity in the case of $mE_{app} \geq 3.94 \times 10^7$ V/cm, with some small dependence on work function, for a diode with a 1in gap.

APPENDIX A : DIMENSIONLESS VARIABLES

Although modern computers can easily handle both very large and very small numbers, it is still considered good programming practice to work with small (≈ 1) numbers whenever possible. To facilitate this, variables (such as time, distance, velocity, etc.) are transformed into dimensionless quantities. The transformation is accomplished by dividing each occurrence of a particular variable by some constant value of the variable relevant to the problem. For example, if one were to examine the motion of billiard balls on a table top, one could divide the masses in the equations of motion by the mass of a single billiard ball m_b , thus reducing the values of the masses to 1 during the computations. After all of the calculations are finished, one would then multiply the dimensionless values by the appropriate constants to get real values.

Since some variables are composites of others (e.g., velocity is composed of distance and time), once a certain number of variables has been transformed, transformation of the remaining ones is then governed by the constants already chosen and the physical equations of the problem at hand. For the billiard ball example, one might choose time, distance, and mass for transformation first. Momentum, force, and energy, since they are composed of the three already transformed variables, would eventually be transformed using the three constants for time, distance, and mass, along with any physical constants which may appear in the governing equations. Often the "base" (non-composite) variables are chosen for transformation first. In this thesis, such base variables would be time, mass, charge, and distance. Indeed, the first three have been chosen here. But rather than distance, current density has been selected instead. Current density was chosen since the graph of current density vs. time was so central in the thesis.

The basic transformations are, then:

$$\begin{array}{llllll}
 \text{time} & : & t & \times & \frac{1}{T} & \rightarrow & \tau ; \\
 \text{mass} & : & M & \times & \frac{1}{M_e} & \rightarrow & \tilde{M} ; \\
 \text{charge} & : & q & \times & \frac{1}{e} & \rightarrow & \tilde{q} ; \\
 \text{current} & & & & & & \\
 \text{density} & : & J & \times & \frac{1}{J_0} & \rightarrow & \tilde{J} .
 \end{array}$$

All other variables can be transformed using the four constants above:

$$\begin{array}{llllll}
 \text{distance} & : & x & \times & \frac{2 \epsilon_0 M_e}{T^3 e J_0} & \rightarrow & \tilde{x} ; \\
 \text{velocity} & : & v & \times & \frac{2 \epsilon_0 M_e}{T^2 e J_0} & \rightarrow & \tilde{v} ; \\
 \text{acceleration} & : & a & \times & \frac{2 \epsilon_0 M_e}{T e J_0} & \rightarrow & \tilde{a} ; \\
 \text{electric} & & & & & & \\
 \text{field} & : & E & \times & \frac{2 \epsilon_0}{T J_0} & \rightarrow & \tilde{E} .
 \end{array}$$

Where

$T \equiv$ time step (s) ;

$M_e \equiv$ electron mass = 9.11×10^{-31} kg ;

$e \equiv$ | electron charge | = 1.60×10^{-19} C ;

$J_0 \equiv$ current density at cathode at $t = 0$ (A/cm²) ; and

$\epsilon_0 \equiv$ permittivity of free space = 8.85×10^{-12} C²/N–m² .

The extra factor of $2 \epsilon_0$ comes from the governing physical equations. This can be seen by looking at the derivation of the transformation of the dimensionless electric field, \tilde{E} . Eq. (13) can be rewritten as

$$E = \frac{J_0 T}{2 \epsilon_0} \sum \frac{J_k}{J_0} \frac{\Delta t}{T} = \frac{J_0 T}{2 \epsilon_0} \sum \tilde{J}_k \Delta \tau. \quad (23)$$

Rearranging gives

$$\frac{2 \epsilon_0}{J_0 T} E = \sum \tilde{J}_k \Delta \tau. \quad (24)$$

As the right side is dimensionless, so must be the left side, and one gets

$$\tilde{E} = \frac{2 \epsilon_0}{J_0 T} E = \sum \tilde{J}_k \Delta \tau. \quad (25)$$

If $\Delta \tau = 1$, as it does in the program,

$$\tilde{E} = \sum \tilde{J}_k. \quad (26)$$

The power of Eq. (26) lies in its simplicity; dimensionless electric fields and current densities become "equivalent." Only addition is required for the calculation of the dimensionless electric field; no program steps are wasted multiplying the dimensionless current densities by constants. As equations of the form of Eq. (26) make up a large part of the computations, the reduction in the number of calculations can be significant.

Since the factor of $2 \epsilon_0$ appears in the expression for the dimensionless electric field, it must also appear in the remaining equations for acceleration, velocity, and distance. From Eq. (22) one can get for the acceleration $a = dv/dt$

$$a = \frac{1}{\gamma^3} \frac{q}{e} \frac{E(2 \epsilon_0)}{J_0 T} \frac{M_e}{M} \left[\frac{e J_0 T}{2 \epsilon_0 M_e} \right] . \quad (27)$$

Rearranging yields

$$\frac{2 \epsilon_0 M_e}{e J_0 T} a = \frac{q E}{\gamma^3 \tilde{M}} . \quad (28)$$

Again, as the right side is dimensionless, so must be the left side, and one gets

$$a = \frac{2 \epsilon_0 M_e}{e J_0 T} a = \frac{q E}{\gamma^3 \tilde{M}} . \quad (29)$$

Interestingly enough, since $\tilde{q} = \tilde{M} = 1$ in the program, acceleration, almost like current density, is nearly "equivalent" to the electric field in dimensionless form.

Velocity and distance are related to acceleration by factors of $(1/T)$ and $(1/T)^2$, respectively:

$$v = \frac{2 \epsilon_0 M_e}{e J_0 T^2} v ; \quad \bar{x} = \frac{2 \epsilon_0 M_e}{e J_0 T^3} x . \quad (30)$$

APPENDIX B : SIMULATION PROGRAM

```
/* Variable Parameters */
```

```
#include <stdio.h>
#include <cmath.h>
#include <greeks.c>
```

```
#define RUN          100000      /* array size */
#define dt           1          /* time step (dimensionless) */
#define T            1.0E-17    /* time step (sec) */
#define GAP          2.54       /* gap size (cm) */
#define m            100        /* enhancement factor */
#define wkfun         4.0        /* work function (eV) */
#define Eapp          3.94E6     /* applied E-field (V/cm) */
#define yscale        1000      /* for plotting */
#define MAX           1.1       /* plot all pts. w/y-val.>MAX */
#define mult          1         /* plot limit/mult pts. */
#define hunch         3.0       /* artificial charge est. */
#define limit         800       /* # of run steps */
```

```
/* Declarations and Assignment of Initial Values */
```

```
main()  
{  
    double  E[RUN+1],J[RUN+1],x[RUN+1],v[RUN+1],a[RUN+1],F,  
            Jmult,gapdist,dx,xmin,xmax,ymin,ymax,lablxmin,  
            lablxmax,lablymin,lablymax,ploty[RUN+1],Ffact,  
            Jfact,Jexpfact,c2,alpha,gammainv,spchrg;  
  
    int  c,f,i,j,k,l,p,q,t,oldest,n,pmult,ixmin,ixmax,  
        iymin,iymax,plotx[RUN +1],mark,iy,flag,ily;  
  
    pmult = mult;  
  
    Jexpfact = (-6.42E7)*pow(wkfun,1.5);  
  
    F = m*Eapp;  
  
    J[0] = ((1.54E-6)*F*F/wkfun)*exp(Jexpfact/F);  
  
    Ffact = m*T*J[0]/(2.0*(8.85E-14));  
    Jfact = (1.54E-6)/(wkfun*J[0]);  
  
    E[0] = Eapp*2.0*(8.85E-14)/(T*J[0]);  
  
    alpha = (1.0E-6)*2.0*(8.85E-12)*(9.11E-31)/  
            (T*T*T*(1.6E-19)*J[0]);  
  
    gapdist = alpha*GAP;  
  
    x[0] = 0.0;  
    v[0] = 0.0;  
  
    c2 = alpha*T*(3.0E10)*alpha*T*(3.0E10);  
  
    oldest = 1;  
    t = 1;  
    mark = 1;  
    c = 1;  
    flag = 0;  
    f = 0;  
    spchrg = hunch;  
    ymin = -0.001;
```

```
/* Determine Electric Fields, Accelerations, Velocities, and
Positions for Existing Disks; Eliminate Disks at Anode */
```

```
while(t <= limit)
{
    for(i = oldest; i <= (mark-1); i = i +1)
    {

        if(i != oldest)
            E[i] = E[i-1] - J[i-1] - J[i];

        gammainv = sqrt(1.0-(v[i]*v[i]/c2));
        a[i] = E[i]*gammainv*gammainv*gammainv;
        v[i] = v[i] + a[i]*dt;
        x[i] = x[i] + v[i]*dt;

        if(x[i] >= gapdist)
        {
            oldest = oldest + 1;

            for(j = oldest; j <= (mark-1); j = j+1)
                E[j] = E[j] + J[oldest - 1];
        }
    }
}
```

```

/* Determine Electric Fields, Velocity, Position, and
Current Densities for Newly Created Disks at Cathode;
Decrease Artificial Space Charge */

```

```

    if(flag==0)
        E[mark] = E[0] - spchrg;

    else
        E[mark] = E[0];

    x[mark] = x[0];
    v[mark] = v[0];

    for(k = oldest; k <= (mark-1); k= k+1)
        E[mark] = E[mark] - J[k];

    F = Ffact*E[mark];

    J[mark] = Jfact*F*F*exp(Jexpfact/F);

    spchrg = spchrg - J[1];

    if(spchrg<0.0 && flag == 0)
    {
        flag = 1;
        f = t;
    }

```

```

/* Determine Points for Plotting; Calculate Electric
Field Changes Due to Newly Created Disk at Cathode;
Increment Time Step */

```

```

    if (t==pmult)
    {
        plotx[c] = t;
        ploty[c] = log10(J[mark]);
        c = c+1;
        pmult = pmult + mult;
    }

else if (J[mark]>MAX)
    {
        plotx[c] = t;
        ploty[c] = log10(J[mark]);
        c = c+1;
    }

if (log10(J[mark])<ymin)
    ymin = log10(J[mark]);

for (l = oldest; l <= (mark-1); l = l+1)
    E[l] = E[l] + J[mark];

t = t + dt;

mark = mark + dt;

```



```
/* "Recycle" Arrays if Full; End While Loop */
```

```
    if (mark > RUN && RUN != limit)
    {
        for (q = oldest; q <= RUN; q = q + 1)
        {
            E[q - oldest + 1] = E[q];
            J[q - oldest + 1] = J[q];

            a[q - oldest + 1] = a[q];
            v[q - oldest + 1] = v[q];
            x[q - oldest + 1] = x[q];
        }

        mark = RUN - oldest + 2;
        oldest = 1;
    }
}
```

```

/* Setup Graphics */

ymax = 0.0;

ixmin = 0;
ixmax = limit;

iymin = (int)(ymin*yscale);
ymax = (int)(ymax*yscale);

lablxmin = 0.0;
lablxmax = T*limit;

lablymin = ymin;
lablymax = 0.0;

/*****/
init();
color_scale("cyanblue");
grey_scale("greyscale1"); window0();
bgcol(7); erase(); color(0);

move(245,30);printf("Log Current Density Ratio vs. Time");
move(75,384);printf("Log J/J");size(1,1);sub('0');
size(2,2);
move(435,700);printf("Time (sec)");

move(85,96);printf("%-3.2f",lablymax);
move(85,660);printf("%-3.2f",lablymin);
move(195,682);printf("%3.2f",lablxmin);
move(760,682);printf("%3.2e",lablxmax);

move(810,150);printf("m = %d",m);
move(810,250);greek(BETA);printf("=%-2.1e",T);
move(810,350);greek(Phi);printf(" = %-2.1f",wkfun);
move(810,450);printf("E");size(1,1);sub('a');sub('p');
sub('p');size(2,2);printf("=%-2.1e",Eapp);
move(810,550);printf("f = %d",f);
move(810,630);printf("old=%d",oldest);

move(350,760);printf("J");size(1,1);sub('0');size(2,2);
printf(" = %4.2e Amp-cm",J[0]);size(1,1);
sup('-');sup('2');size(2,2);

window(224,96,800,672);bgcol(3);erase();
scale(ixmin,ymax,ixmax,iymin);
rect(ixmin,ymax,ixmax,iymin);color(4);
/*****/

```

```

/* Plot Graph of Log Current Density vs Time; End Program */

catvec(ixmin,(int)(log10(J[1])*yscale));

for(p=1;p<c;p=p+1)
    printf("%d,%d,0,plotx[p],(int)(ploty[p]*yscale));

printf(";");

window0();color(0);size(1,1);mode("P0");

iy = 672-(int)((672-96)*((yscale*ploty[p-1])-iymin)/
    (iymax-iymin));

move(805,iy);

printf("%4.3e",ploty[p-1]);

ily = 672-(int)((672-96)*((yscale*ploty[1])-iymin)/
    (iymax-iymin));

move(160,ily);

printf("%4.3e",ploty[1]);

}

```

LIST OF REFERENCES

1. Mesyats, G.A. and Proskurovsky, D.I., *Pulsed Electrical Discharge in Vacuum*, Springer-Verlag, 1989.
2. Schwirzke, F., *Laser Induced Breakdown and High Voltage Induced Vacuum Breakdown on Metal Surfaces*, Laser Interaction and Related Plasma Phenomena, Vol. 9, pp. 335-357, H. Hora and G.H. Miley, eds., Plenum Publishing Corporation, 1991.
3. Hallal, M.P. Jr., *The Onset of Breakdown in a Fast Pulsed Vacuum Diode*, M.S. Thesis, Naval Postgraduate School, Monterey, California, June 1991.
4. Curtiss, D.H., *Theoretical Model of the Cathode Spot in a Unipolar Arc*, M.S. Thesis, Naval Postgraduate School, Monterey, California, December 1987.
5. Morris, E.C.A., *Understanding and Improving the Neutral Beam Injector Conditioning Problem*, Max-Planck-Institut für Plasmaphysik IPP 4/250, September 1991.
6. Parker, R.K., *Explosive Electron Emission and the Characteristics of High-Current Electron Flow*, Air Force Weapons Laboratory Technical Report AFWL-TR-73-92, February 1974.
7. Miller, R.B., *An Introduction to the Physics of Intense Charged Particle Beams*, Plenum Press, 1982.
8. Birdsall, C.K., *Particle-in-Cell Charged-Particle Simulations, Plus Monte Carlo Collisions With Neutral Atoms*, PLC-MCC, IEEE Transactions on Plasma Science, Vol. 19, No. 2, pp. 65-85, April 1991.

INITIAL DISTRIBUTION LIST

- | | | |
|----|---|---|
| 1. | Defense Technical Information Center
Cameron Station
Alexandria, VA 22304-6145 | 2 |
| 2. | Library, Code 52
Naval Postgraduate School
Monterey, CA 93943-5002 | 2 |
| 3. | Professor Fred Schwirzke, Code PH/Sw
Department of Physics
Naval Postgraduate School
Monterey, CA 93943-5000 | 3 |
| 4. | Professor William B. Colson, Code PH/Cw
Department of Physics
Naval Postgraduate School
Monterey, CA 93943-5000 | 1 |
| 5. | Professor Karlheinz E. Woehler, Code PH/Wh
Chairman, Department of Physics
Naval Postgraduate School
Monterey, CA 93943-5000 | 1 |
| 6. | Physics Library, Code PH
Department of Physics
Naval Postgraduate School
Monterey, CA 93943-5000 | 1 |
| 7. | LT David S. Welsh
4166 Robin Hood Drive
York, PA 17404-9421 | 2 |

144-403

Thesis

W4455 Welsh

c.1 Current density limitations in a fast-pulsed high-voltage vacuum diode.

Thesis

W4455 Welsh

c.1 Current density limitations in a fast-pulsed high-voltage vacuum diode.

DUDLEY KNOX LIBRARY



3 2768 00036286 7